POLITECNICO DI TORINO

Master of science degree in Mechatronic Engineering

Master's degree thesis

A Respiration Rate-based algorithm for drowsiness detection

Politecnico di Torino

Supervisor:
prof. Massimo Violante

Candidate:
Marika Tieni

Co-Supervisor:
prof. Luigi Pugliese

December 2021

Abstract

Drowsy driving can lead to road accidents. Therefore, it is essential to find methods to prevent drowsy driving.
The aim of this thesis is the implementation of a method for detecting drowsy driving using the respiration rate (RR).
Data have been collected through a dynamic driving simulator. RR data has been measured with a thoracic respiratory band for the Polysomnographic test.
Two real-time algorithms have been developed to detect drowsy driving from the dsRR (differential of the standard deviation of the respiration rate) and the dmRR (differential of the medium value of the respiration rate) of a certain window of RR signal samples.
The needed system transfer functions have been identified through the set-membership identification approach.
The algorithms can predict the first falling asleep in most of the cases.

Table of Contents

List of Figures

List of Tables

Chapter 1

Introduction

One of the most frequent causes of car accidents is drowsiness at the wheel. Drowsiness is responsible of decreasing mental alertness, affecting the individual's ability to drive a vehicle safely and increasing the risk of human error that could lead to accidents.

This thesis proposes an algorithm for drowsiness detection through the respiration rate (RR) signal analysis.
The required data have been acquired through the Polysomnography (PSG) test and the power spectrum analysis of the Photoplethysmogram (PPG) signal.

In this thesis, the following principal chapters will be examined:

- **State of the art**: in this chapter, the influence of sleepiness on road accidents and the main methods to contain the problem will be briefly presented. The sleep cycle, PSG analysis and PPG signal will also be analysed.

- **Driver drowsiness dataset**: in this chapter, the dataset used for the identification of the system and finally for the development of the sleep prediction algorithm will be presented.

- **Methodology**: in this chapter, the set-membership identification approach for system identification will be applied and the development of the drowsiness detection algorithm will be explained.

- **Analysis of the results**: in this chapter, the results of the algorithm will be analysed in terms of sleep prediction time, sensitivity and specificity.

Chapter 2

State of the art

2.1 Driver drowsiness and road accident

Driver drowsiness is a major case of road accident. Indeed, according to the American National Highway Traffic Safety Administration (NHTSA), falling asleep is the most influential factor in the fatal single vehicle road crashes, followed by other causes such as alcohol use and vehicle speed. Depending on the considered country, a percentage between 5% and 25% of fatal road accident involved driver sleepiness [1].

In addition, according to some studies [2], two hours of continuous nocturnal driving produce a driving impairment compatible with a blood alcohol concentration of 0.05%.
Furthermore, drivers with sleep disorders and sleepless are more prone to have road accidents.

An Internet survey [3] regarding traffic incident experiences investigates on the psychosomatic states before traffic incidents. The result of this survey is shown in the following *Figure 2.1*. As it can be noticed, the psychosomatic states before traffic incident were identified as haste (22%), distraction (21.9%), inexperienced driving (7.6%) and drowsy driving (3.8%). Thus, the drowsiness of a driver is one of the potential factors that can cause road accidents.

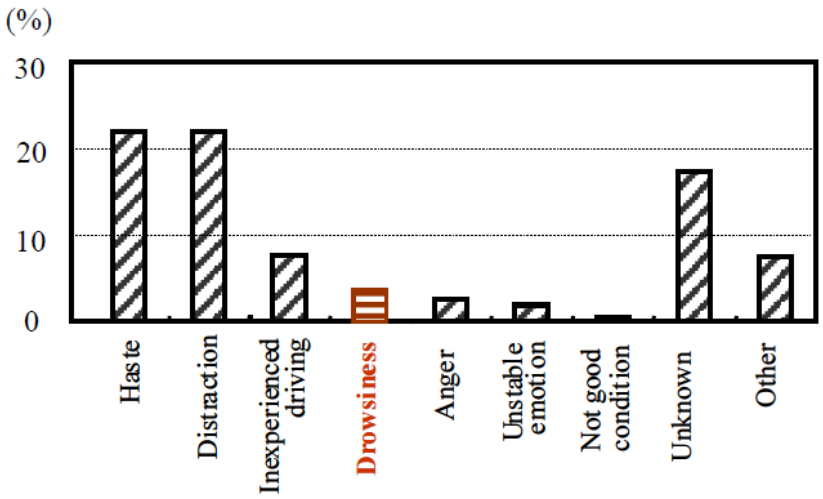

Figure 2.1: Psychosomatic state of the driver before road accident [14]

Therefore, finding methods to prevent drowsy driving and related accidents is crucial to improve road safety.

2.2 Methods to prevent drowsy driving

In order to reduce road accidents related to driver drowsiness or fatigue, different types of measures could be taken.

An example of practical measures are shelters for sleepy drivers installed on the highway in South Korea (*Figure 2.2*). This rest-stop measure decreased the number of accidents by 28% and the number of deaths by 55% [4].
Nevertheless, the drawback of this countermeasure is that the non-highways are not equipped with such rest areas for sleepy drivers.

Figure 2.2: Shelters for sleepy drivers

In recent years, measures for accurate drowsiness detection have been subject of studies. According to some of these studies [5], such measures include vehicle-based measures, behavioural measures, and physiological measures.

- **Vehicle-based measures** depend on the vehicle velocity, acceleration, wheel position, etc.. These measures are non-invasive and relatively accurate, but they are highly dependent on driver's driving skills, road conditions, vehicle characteristics. Another drawback is the potential risk of taking time for detecting the vehicle motion in real driving scenario.
  PLK Technology developed the first lane departure warning system (LDWS), employed for the first time in the world by Hyundai [4].
  Volvo developed a system able to detect deviations from the driving lane using a camera connected to the LDWS (*Figure 2.3*).

Figure 2.3: LDWS working principle

Mercedes-Benz also developed a drowsy driving detection system that memorizes each driver's driving patterns in the first 20 minutes of driving and enables operation in the range 80–180 km/h.

- **Behavioural measures** are based on the usage of camera to detect driver's eye state, eye blinking rate, yawning, head movement, etc. (*Figure 2.4*). These measures have the advantage of being easy to use but they are sensitive to camera movement, surrounding environment, lighting conditions.

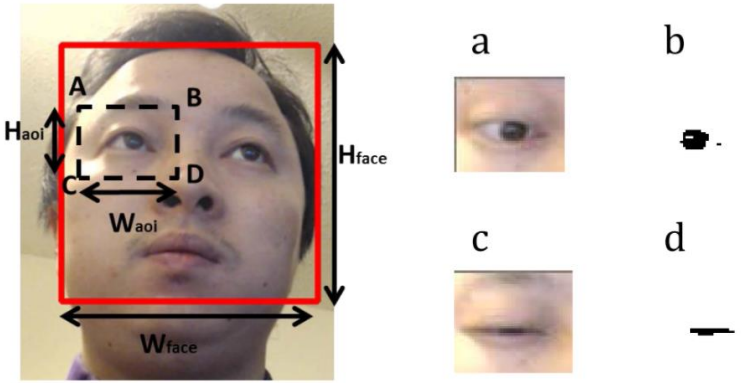

Figure 2.4: Blink detection [18]

- **Physiological measures** are an alternative or complement means to vehicle-based and behavioural measures. Physiological measures are based on biometrical signals such as heart rate, brain activity, respiration. These signals are acquired with different sensors: electrocardiogram (ECG), electroencephalogram (EEG), photoplethysmogram (PPG), etc. [5].

2.3 Recent studies on driver drowsiness detection

The correlation between bio-signals and driver drowsiness has been subject of several studies.

Some studies showed that drowsiness is associated with changes in eye movement, heart and respiration rates, and EEG [4].

A Korean study [4] confirmed the correlation between the drowsiness and the higher frequency of blinks together with the longer duration of eye closure. A drowsiness perception system able to judge drowsiness through a vision system was developed. The vision system allowed to detect the eye region, the eye blinking frequency and the eye closure duration. Finally, a detection algorithm was developed to associate these two variables with the drowsiness state.

Kim et al. [4] analysed the drowsy driving detection through a sensor system based on respiration (*Figure 2.5*). This system was a piezoelectric pressure sensor used for the measurement of pressure variations induced by the movement of the driver abdomen during breathing. Their analysis results indicated that the

respiration peak of a driver in a state of drowsiness is at least 83% lower with respect to the one of an alert driver. In addition, the respiration rate is at least 10% higher [4].

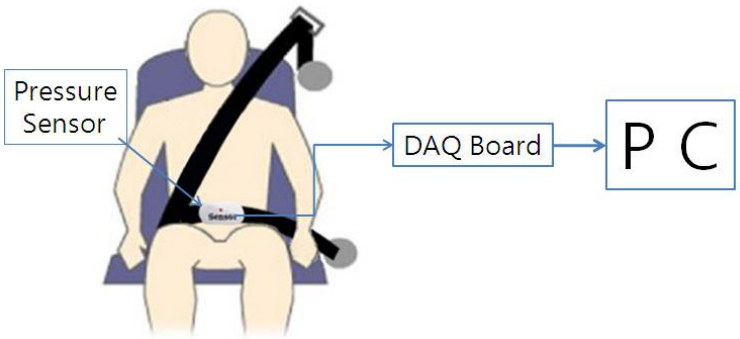

Figure 2.5: Experiment setting [4]

Moon et al. [6] implemented an algorithm able to detect drowsy driving based on jerking patterns using a steering angle sensor [4].

In the following, the characteristics of ECG and PPG signals and their correlation with heart activity are discussed. Afterwards, the correlation between bio-signals and drowsiness will be analyzed.

2.4 Biological background

2.4.1 Heart physiology

The heart is responsible for rhythmically pumping blood in the body, allowing the transport of vital nutrients and oxygen to the cells. The heart is divided into four chambers with different functions (*Figure 2.6*).

The chambers on the right side, the right atrium and right ventricle, are responsible for delivering deoxygenated blood through the pulmonary circulation. The chambers on the left side, the left atrium and the left ventricle, deliver oxygenated blood through the systemic circulation.

This vital function is accomplished by the cardiac muscle when electrically stimulated by the Central Nervous System (CNS). The electrical stimulation consists of a wave of electrical current conducted through a complex network of cardiac muscle fibres before every heartbeat. This phenomenon produces potential

differences on the body surface that can be measured with specific surface electrodes and acquisition hardware. The resulting graphical recording of the potential difference signals is known as Electrocardiogram (ECG) [7].

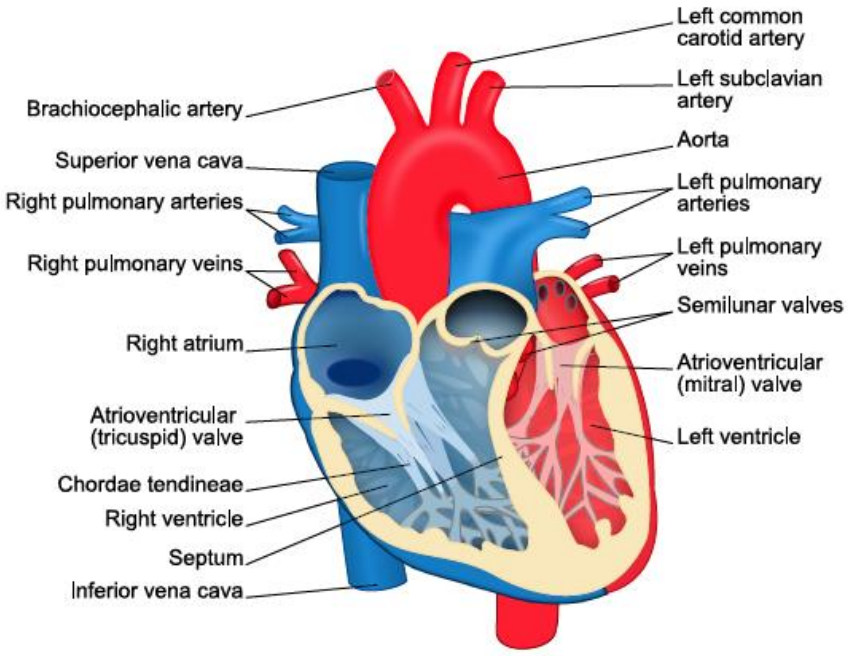

Figure 2.6: Heart physiology

In normal condition, the heart is stimulated by the SA node, situated in the right atrium at the superior vena cava (*Figure 2.7*). This node activates the muscular cells of the right atrium. Then, this electrical wave propagates also activating the rest of the atria.

The Atrioventricular (AV) node is located at the boundary between the atria and ventricles. This node is responsible of propagating the activation wave to the ventricles and provides the only path for the electrical waves, since the atria and the ventricles are separated by an insulating fibrous barrier.

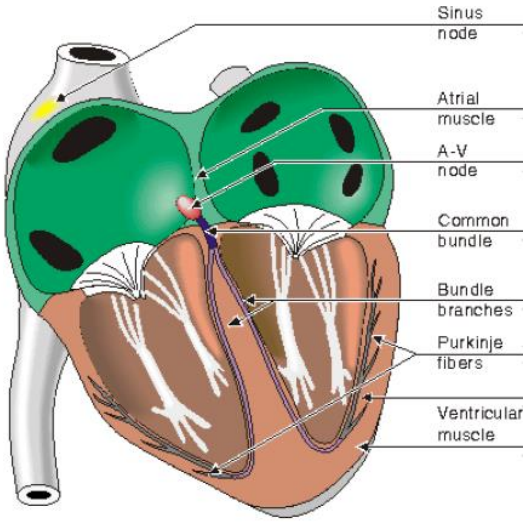

Figure 2.7: Normal ECG shape

Therefore, the SA node acts as the primary pacemaker of the heart and is responsible of setting the working frequency of the heart HR. The SA node activity is regulated by the CNS, more specifically by the Autonomous Nervous System (ANS). The ANS regulates the activity of certain organs (heart, digestive tract, lungs, bladder and blood vessels). It is also known as the involuntary motor system since most of these functions happen unconsciously.

The ANS is composed of two subsystems: the sympathetic and parasympathetic nervous systems. These two branches are responsible of different and opposite tasks.

The sympathetic nervous system, also known as the “fight or flight” system, is activated during physically or mentally stressful situations. Its activity causes an increment of the SA stimulation resulting in an increase of the depolarization wave propagation velocity and then of the HR raising.

The parasympathetic nervous system, also known as the “rest and digest” system, aims to slow down the HR.

As previously discussed, sympathetic and parasympathetic systems have opposite tasks. Nevertheless, their interaction is not competing rather than complementary. This continuous modulation by the vagal and sympathetic branches is known as sympathovagal balance.

The Heart Rate Variability (HRV) is the oscillation in the interval between consecutive heartbeats. Since the HR variations are consequences of the sympathovagal balance, the HRV is an important indicator of the ANS activity through the SA node. Therefore, the variability in the heartbeat periods is connected to the sympathovagal balance.

The HRV time series can be obtained through the ECG or PPG recording [7]. This will be the subject of the next chapters, but first a general overview of sleep stages and their correlation with ANS activity will be given.

2.4.2 The sleep cycle

Sleep is an important factor for the health of human organism. Sleeping takes up about a third of human existence, representing one of the main activities of a human being's life. It is a state of apparent quietness in which the organism works to rest, eliminate toxins and strengthen cognitive functions, including memory.

Normally, people sleep on average 8 hours. Nevertheless, sleep is not uniform. Over the course of the night, the total sleep is made up of several cycles, which are composed by the two macro-moments NREM (Non-Rapid Eye Movement) and REM (Rapid Eye Movement).
In a typical night, a person completes on average 5 cycles. Not all sleep cycles have the same length, but on average they last about 90 minutes each. However, depending on the person, this can vary between 80-120 minutes.
Therefore, sleep is characterised by a cyclical alternation of about five cycles, which are in turn divided into two macro-moments: NREM and REM. NREM has 3 stages whereas REM has a unique stage.

During sleep, a person usually progresses through the 3 stages of NREM before entering REM sleep. The NREM and REM last approximately 60-70 and 15 minutes, respectively. However, their duration may vary, as shown in the following *Table 1*:

Sleep Stages	Type of Sleep	Other Names	Normal Length
Stage 1	NREM	N1	1-5 minutes
Stage 2	NREM	N2	10-60 minutes
Stage 3	NREM	N3, Slow-Wave Sleep (SWS), Delta Sleep, Deep Sleep	20-40 minutes
Stage 4	REM	REM Sleep	10-60 minutes

Table 2.1: NREM and REM stages and durations [8]

As previously discussed, the first macro-phase of sleep is the NREM phase, which lasts about 75% of the total sleep. It is composed by the following three stages and in the transition from one stage to the next one, sleep becomes deeper and deeper (*Figure 2.8*):

- in the first stage, the body passes from the wakefulness to the sleep state. It is characterised by the lowering of body temperature, the partial relaxation of muscles (the muscles are not yet fully relaxed) and the slowing of the heartbeat. In addition, eye movements are not rapid, a sign that brain activity is slowly decreasing. Since it involves light sleep, it is easy to wake up.
- in the second stage, the heart rate continues to slow down, muscles are completely relaxed, and breathing is very deep.
- the third stage is the deep sleep stage. Here, the eye movement is very slow and body temperature drops further. This is the NREM phase in which the body regenerates and metabolic reserves are restored. There could be body movements and it is very difficult to wake up.

The REM phase is deeper with respect to NREM phases. During REM sleep, the eyes begin to move rapidly (for this reason is called Rapid Eye Movement). In this stage, dreams occur, accompanied by a gradual but noticeable increase in blood flow, respiration, and brain activity. In addition, breathing becomes irregular and apnoea episodes can occur. Moreover, one of the characteristics of this phase is that the muscles of the legs and arms are paralysed [8], [9], [10].

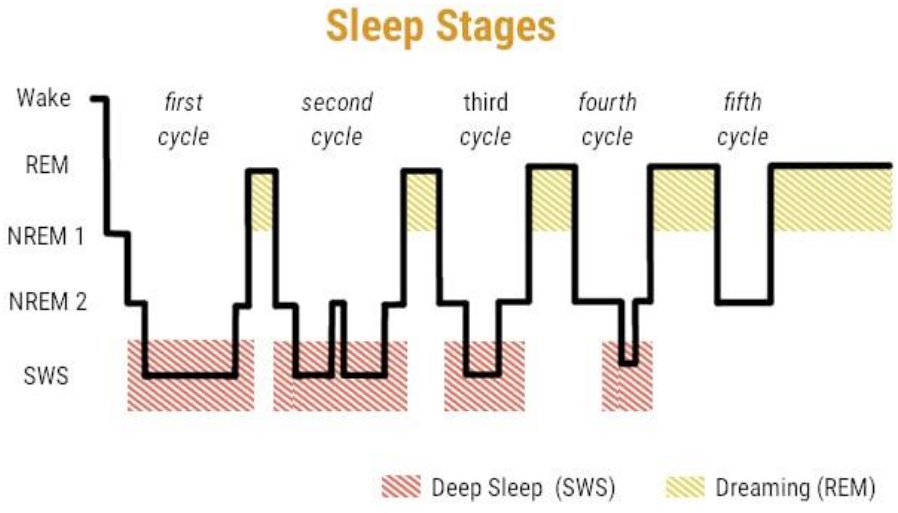

Figure 2.8: Sleep stages [9]

REM and NREM phases are strongly related with ANS activity. Indeed, during NREM phase parasympathetic activity is dominant, whereas, during REM phase is present a strong sympathetic activity.

2.5 The electrocardiogram (ECG)

2.5.1 The ECG test

The electrocardiogram (ECG) is a not-invasive test used to check heart's rhythm and electrical activity. Some sensors (electrodes) are attached to the chest, arms, and legs. These electrodes detect the electrical currents generated by the heart, which are measured and recorded using an electrocardiograph (*Figure 2.9*).

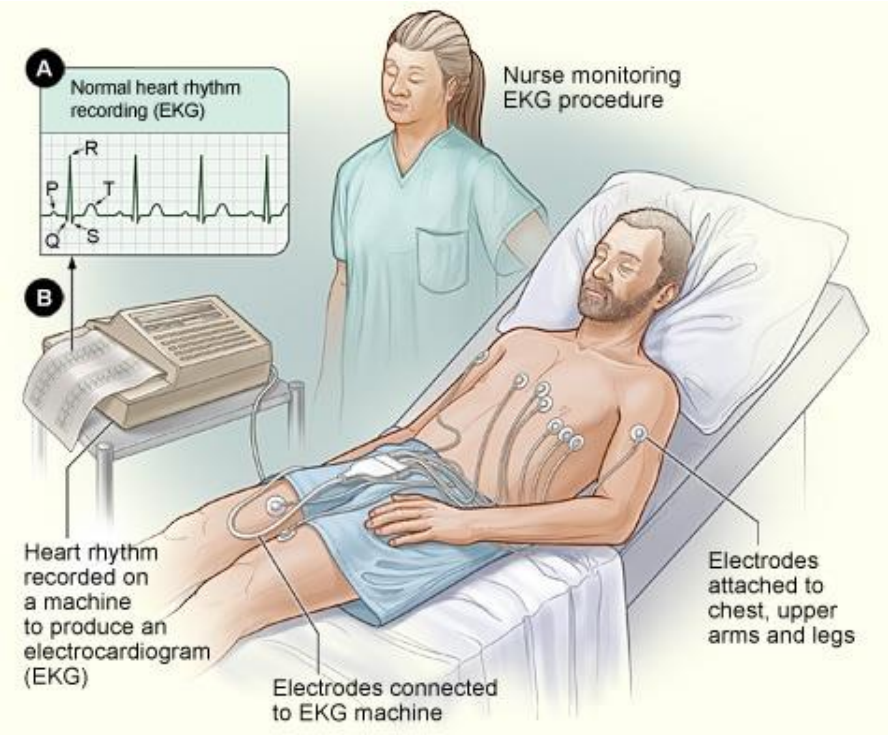

Figure 2.9: The ECG setting

The result of this process is a voltage over time graph representing the electrical activity of the heart (*Figure 2.10*).

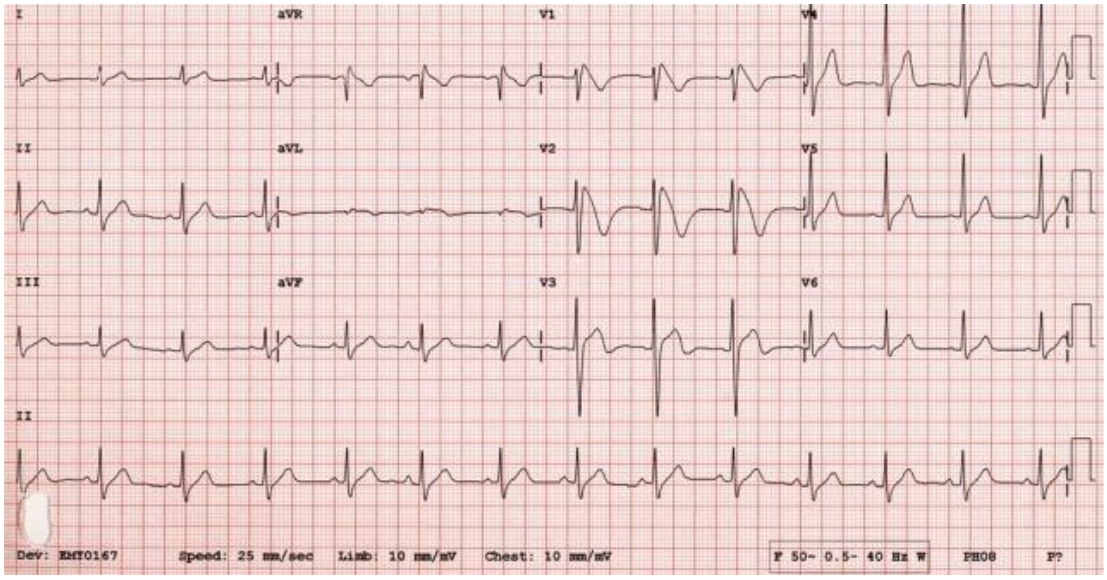

Figure 2.10: An example of electrocardiography

There are three types of ECG:

- **resting ECG** – performed with the patient in a comfortable position. The duration of this test is about 5-10 minutes. Since electrical impulses generated by other muscle movements may interfere with those generated by the heart, patient cannot move during the test

- **ambulatory ECG** – electrodes are connected to a small device. This device records heart activity for at least 24 hours. Patient can move normally during such test. Ambulatory ECG is used for intermittent (start-stop) symptoms that cannot be evaluated through a resting ECG. Patient writes down the episodes in a diary, to compare symptoms with ECG

- **exercise stress test (EST)** – during this type of ECG, patient uses an exercise bike or treadmill. This test lasts about 15 to 30 minutes [11], [12].

2.5.2 The ECG signal

Therefore, the ECG signal is the graphical representation of the potential differences on the thorax surface during the electrical heart activity.

The most common ECG waveform is shown in *Figure 2.11*. However, this shape can vary among healthy patients and depends on the state of health. This wave is divided into three intervals: the P-wave, the QRS complex and the T-wave. Each

of these waves corresponds to specific and sequential events along the electrical pathway.

The P-wave represents the depolarization of the atria before the atrial contraction. This wave is characterized by a low amplitude due to the small amount of muscle in the atria.

The QRS complex corresponds to the atrial repolarization and the ventricular depolarization.

The T-wave represents the ventricular repolarization.

The systole period corresponds to the ventricular contraction phase; the diastole period corresponds to the time interval between ventricular contractions [62].

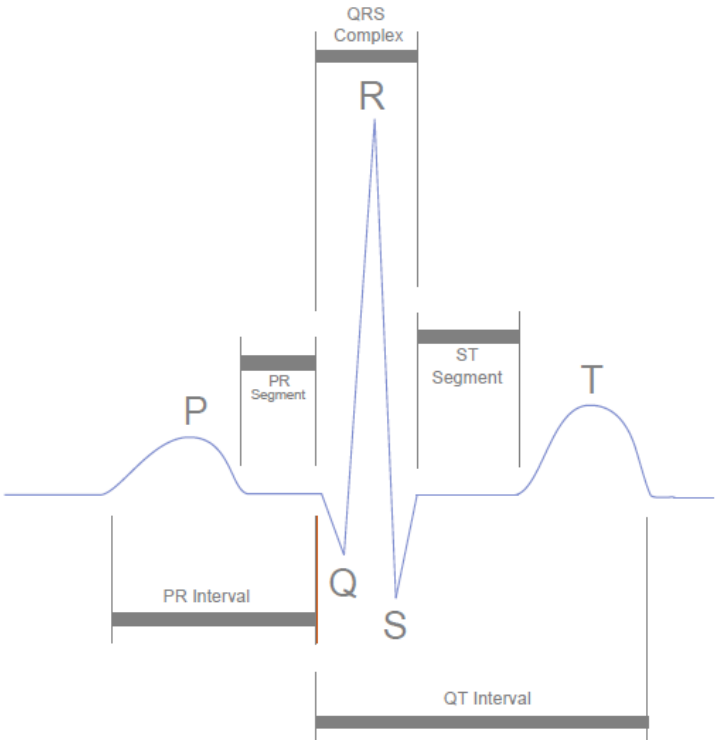

Figure 2.11: Normal ECG shape

The HRV time series can be derived from the ECG recording. The R peak of the QRS complex can be considered to extrapolate the heartbeats. Consequently, the heartbeat period is defined as the time difference between consecutive R peak, as shown in *Figure 2.12.* This interval is known as inter-beat interval, or RR interval.

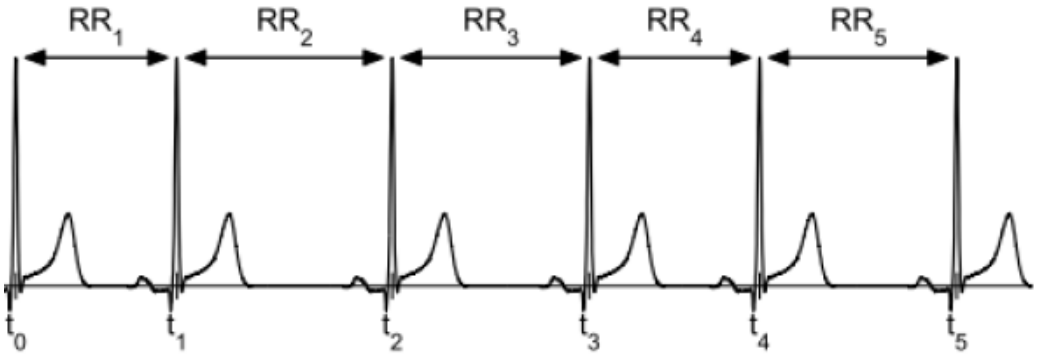

Figure 2.12: RR intervals derivation from ECG

Therefore, the HRV time series are derived, obtaining the interval tachogram (*Figure 2.13*).

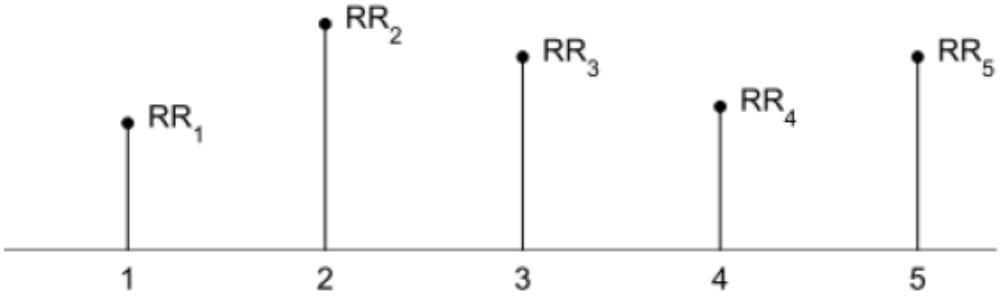

Figure 2.13: Interval tachogram

Finally, the RR intervals are interpolated (linear or cubic interpolation), obtaining the HRV signal. This interpolation step is essential in the case of frequency domain analysis, while is optional for the time domain analysis (*Figure 2.14*).

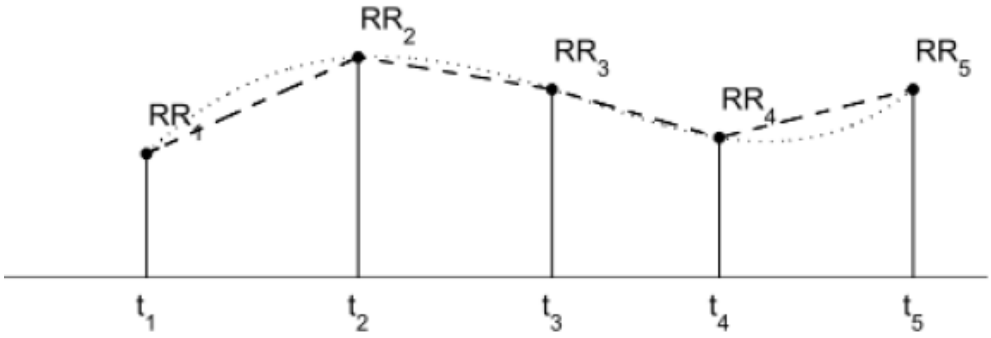

Figure 2.14: Interpolated RR interval series

2.5.3 HRV from ECG drawbacks

The ECG signals are a powerful tool to detect the HRV signal. Nevertheless, there are some inconveniences associated with the ECG recording and the signal detection.

Firstly, the ECG recording requires complicated setups, with large dimensions and people are generally reluctant to use ECG sensors in real driving situations.

Another problem is related to the noise and signal artifacts associated with such recording [62].

To overcome these problems, many researchers give as an alternative the use of Photoplethysmography (PPG). PPG is a sufficiently precise alternative tool to measure HR fluctuations.

2.6 The Photoplethysmography (PPG)

2.6.1 The Photoplethysmography (PPG) test

Photoplethysmography (PPG) is an optical technique used to detect blood volumetric changes in the microvascular bed of tissue. This technique provides information related to the cardiovascular system.

It is a low-cost and non-invasive method that performs measurements at the surface of the skin. A PPG is usually obtained through a pulse oximeter (*Figure 2.15*). This device illuminates the skin and measures light absorption changes.

Figure 2.15: Pulse oximeter

A low-intensity infrared (IR) light travels through biological tissues. This light is absorbed by bones, skin pigments and both venous and arterial blood (*Figure 2.16*).
The light is more absorbed by blood with respect to the surrounding tissues. Therefore, the changes in blood flow are detected by PPG sensors as changes in the intensity of light. Blood flow variations mostly occur in the arteries and not in the veins.
The quantity of blood flowing through the blood vessels is proportional to the voltage signal from PPG.

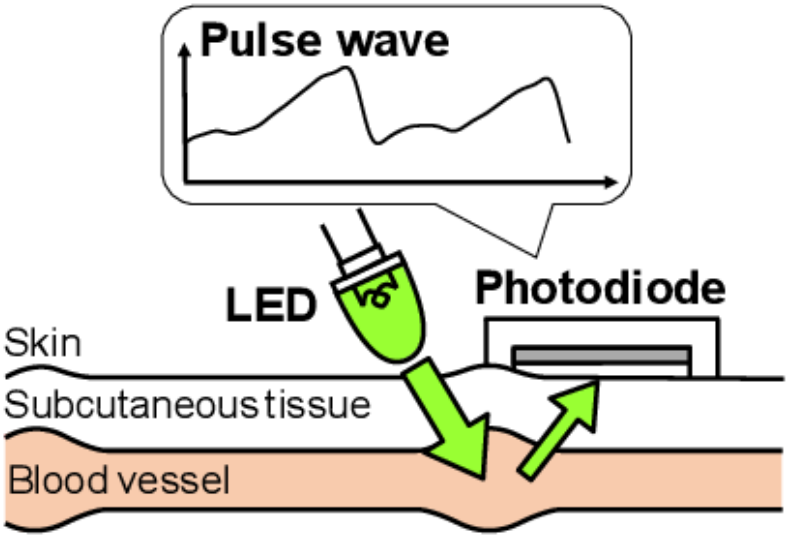

Figure 2.16: PPG working principle

2.6.2 The Photoplethysmography (PPG) signal

As previously described, PPG is an optical measurement technique. During each cardiac cycle, PPG measures the blood volume changes in a specific part of the body (fingertip and earlobe). This technique is based on the optical properties of the tissues. When tissues get illuminated by a light with a specific wavelength, they absorb or transmit or reflect that light depending on the blood volume in the vessels.

The blood volume is related to the cardiac cycle. The cardiac cycle is characterized by two main components: the systole and the diastole.

During the systole period, the heart contracts and expels the arterial blood. In the diastole period, the heart is relaxed and receives blood from veins.

Therefore, these periods correspond to a different quantity of blood level and, consequently, to different levels of light detection.

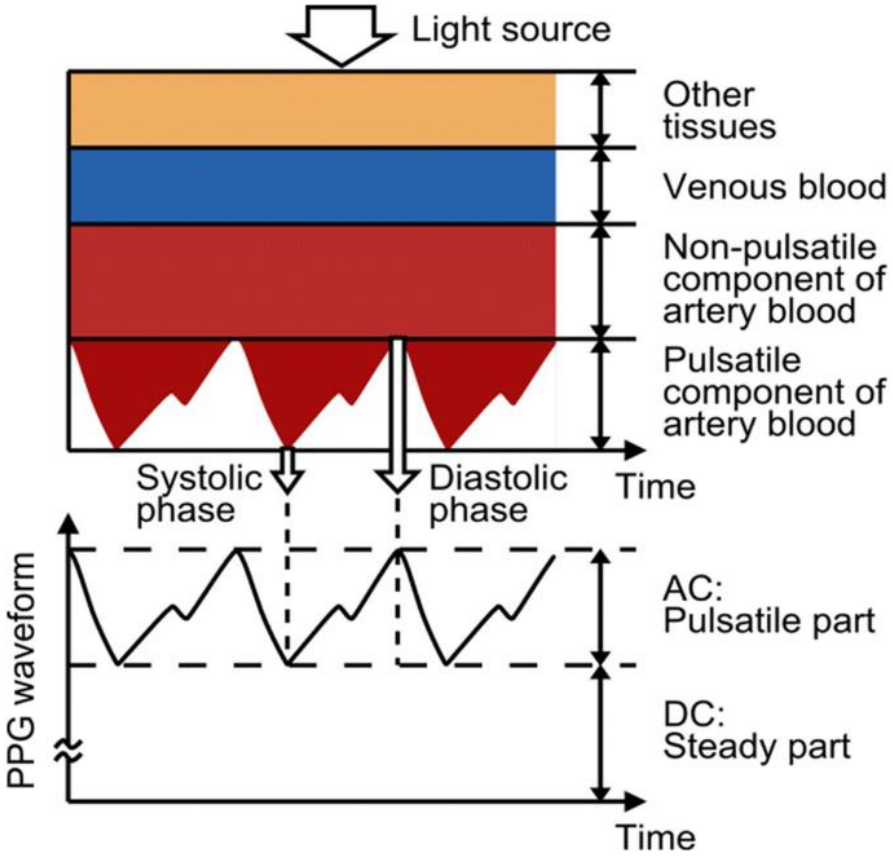

Figure 2.17: PPG waveform and systolic – diastolic phases

The PPG signal is characterized by two components: a small pulsatile AC component and a large non-pulsatile DC component, as shown in *Figure 2.18*.

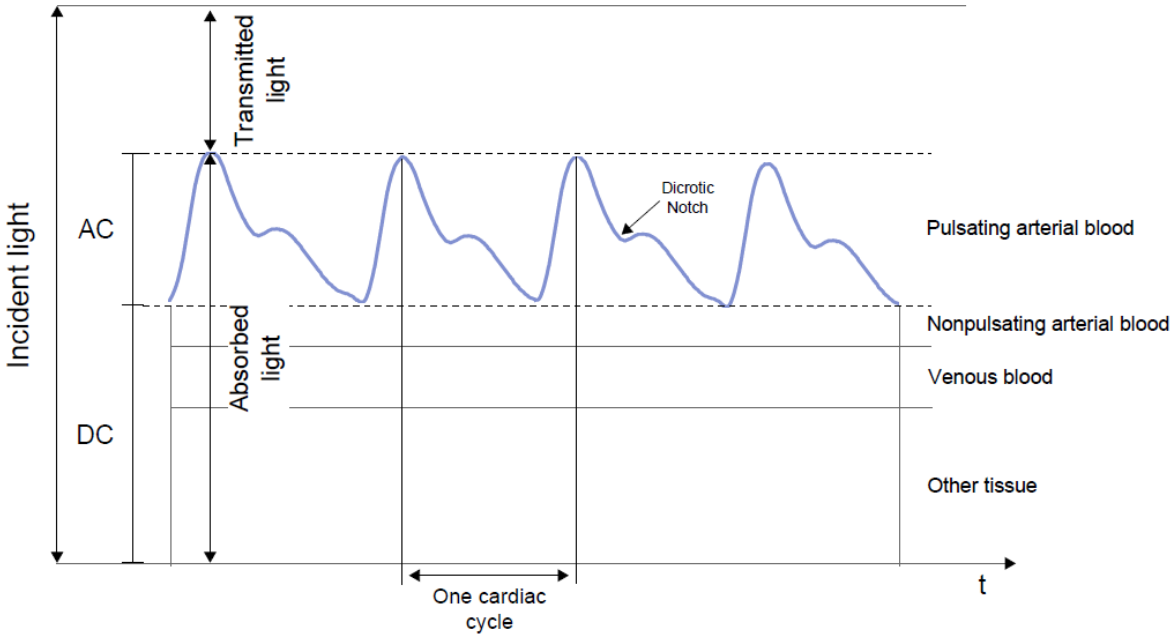

Figure 2.18: Schematic illustration of a photoplethysmogram

The AC component is a consequence of the pulsatile blood, while the DC component is due to absorbance in the tissues, bones, venous blood and non-pulsatile arterial blood. Since sensors have low-pass filters, normally the DC component is removed and only the AC component is shown.

The peaks of the PPG signal correspond to systoles, while the valleys to diastoles, as shown in the following *Figure 2.19*.

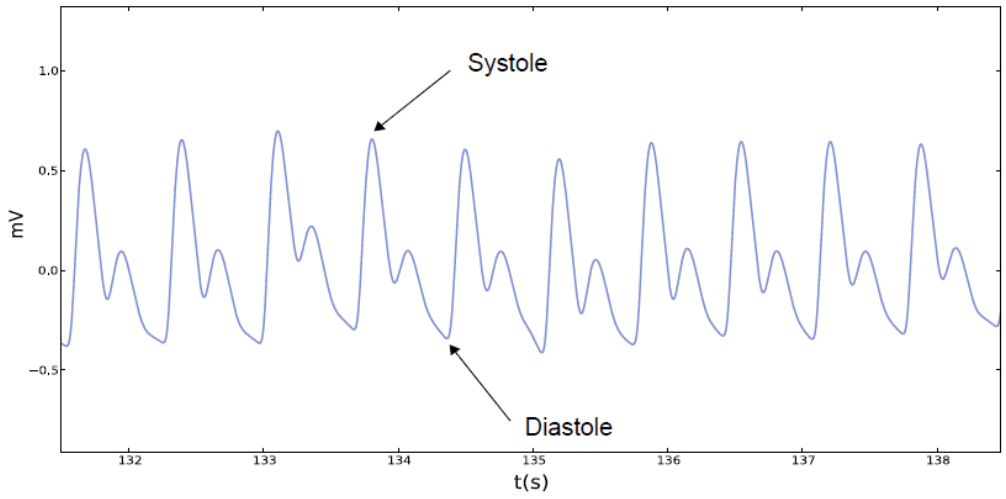

Figure 2.19: Systole and diastole periods in PPG signal

Since the PPG signal reflects the blood volume variations during each cardiac cycle, it may be also correlated with the HRV. Such link between the PPG signal and the HRV can be derived considering consecutive systoles (and not consecutive R peaks, as it was done in ECG signal).

Some studies have been carried and confirmed the correlation between the HRV parameters simultaneously acquired from ECG and PPG.

Therefore, an alternative way for HRV derivation is given by PPG signal. This measure is less obtrusive and more user friendly with respect to ECG sensor. More precisely, PPG sensors represent a small, simple, and low-cost device useful to monitor the pulse rate in a non-invasive manner [5].

2.7 Standard of measurements

In the following, the standard methods used in HRV analysis are described. All these methods derive from HRV time series.

There are three different categories:

- time domain methods
- frequency domain methods
- non-linear methods

2.7.1 Time domain methods

Time domain methods are the easiest to be computed since they are taken from the RR series interval directly. They can be further classified into **statistical** and **geometrical** methods. The available geometrical methods cannot be applied to evaluate long recordings whereas statistical methods can be applied both for long and short recordings. Therefore, statistical methods are more flexible.

2.7.1.1 Statistical methods

In the following, statistical measures indices are described.

Mean value of RR intervals

$$\overline{RR} = \frac{1}{N}\sum_{j=1}^{N} RR_j \tag{2.1}$$

where:

- RR_j is the value of *j'th* RR interval
- N is the total number of successive intervals

Mean Heart Rate (bpm)

$$\overline{HR} = \frac{1}{\overline{RR}} \tag{2.2}$$

SDNN

SDNN (ms) is the Standard deviation of the RR interval. It indicates the overall variation in the RR interval series, in short and long term:

$$SDNN = \sqrt{\frac{1}{N-1}\sum_{j=1}^{N}(RR_j - \overline{RR})^2} \tag{2.3}$$

SDANN

SDANN (ms) is the Standard deviation of the average of RR interval in 5 minutes of recording.

$$SDANN = \sqrt{\frac{1}{N-1}\sum_{j=1}^{N}(RR_{5j} - \overline{RR_5})^2} \tag{2.4}$$

where:

- $\overline{RR_5}$ is the average of all the RR intervals averages in 5 minutes
- RR_{5j} is the value of the *j'th* = 5 RR minutes interval average
- N is the total number of the RR intervals in 5 minutes

SDNN index

SDNN index (ms) is the mean of the standard deviation of the RR intervals of all the 5 minutes segments of the entire 24 hours recording.

$$SDNN_{index} = \sqrt{\frac{1}{N}\sum_{j=1}^{N} SDNN_{5j}} \tag{2.5}$$

where:

- $SDNN_{5j}$ is the standard deviation of the *j'th* = 5 minutes RR interval average
- N is the total number of the RR intervals in 5 minutes

SDSD

SDSD (ms) is the Standard deviation of successive RR interval differences.

$$SDSD = \sqrt{E\{\Delta RR_j^2\} - E\{\Delta RR_j\}^2} \tag{2.6}$$

where:

- $\Delta RR_j = RR_j - RR_{j+1}$
- $E\{\Delta RR_j^2\} = \overline{\Delta RR^2}$
- $E\{\Delta RR_j\} = \overline{\Delta RR}$

RMSSD

RMSSD (ms) is the root mean square of successive differences. In stationary RR series:

$$RMSSD = \sqrt{\frac{1}{N-1}\sum_{j=1}^{N-1}(RR_{j+1} - \overline{RR_j})^2} \tag{2.7}$$

Pnn50

Pnn50 is the percentage of the number of interval differences of successive RR intervals greater than 50 ms (NN50).

$$pNN50 = \frac{NN50}{N-1} \times 100\% \tag{2.8}$$

2.7.1.2 Geometrical methods

In the following, also the geometrical measures are described.

HRV triangular index

HRV triangular index is defined as follows:

$$HRV_{index} = \frac{\int D(t)dt}{Y} \tag{2.9}$$

where:

- $D(t)$ is the density distribution
- Y is the maximum of the density distribution

In the following *Figure 2.20*, a schematic representation of this concept is given:

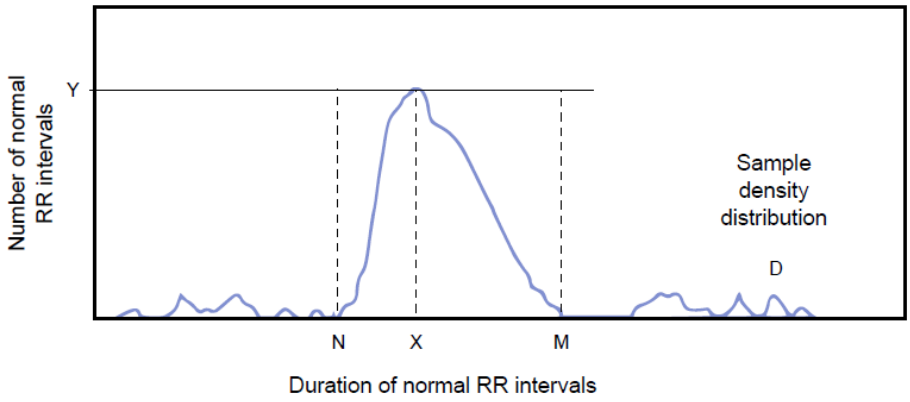

Figure 2.20: Representation of the sample density distribution of a series RR interval [7]

TINN

TINN is the triangular interpolation of the NN interval histogram. Referring to the *Figure* above, NN interval corresponds to the base width of the density distribution. The N and M points are selected to compute TINN. A multilinear function q is also required such that $q(t) = 0$ for $t \leq N$ and $q(X) = Y$ for $t \geq M$. q is introduced in order to obtain the minimum value of the integral $\int_0^{+\infty} \big(D(t) - q(t)\big)^2 dt$.

Therefore, TINN is expressed as:

$$TINN = M - N \tag{2.10}$$

2.7.2 Frequency domain methods

The RR intervals variability affects a wide number of time scales. For this reason, the tachogram's spectral analysis is an interesting tool for analysing factors that contribute to the different components.

The most common power spectral estimation technique for HRV analysis is the Power Spectral Density (PSD) estimation (*Figure 2.21*).

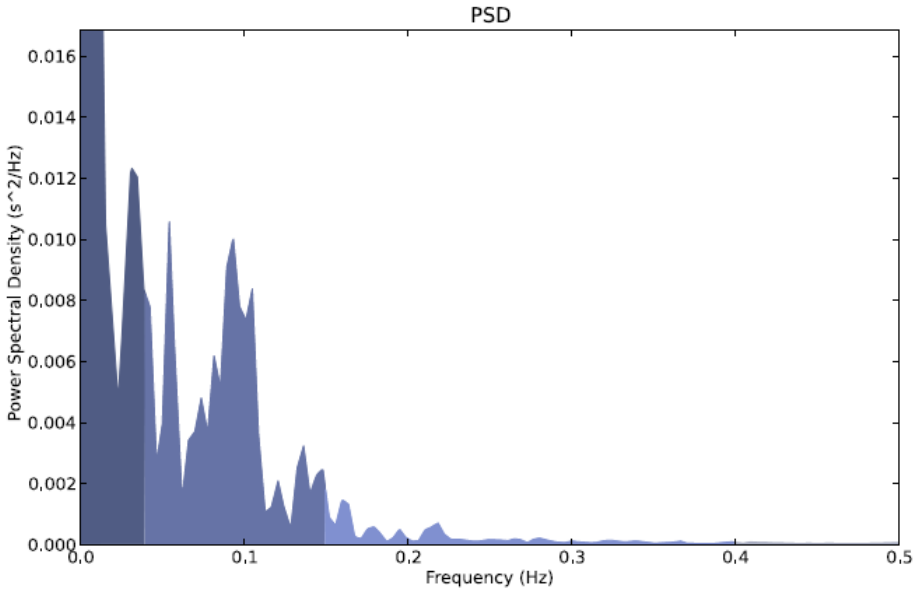

Figure 2.21: PSD example [7]

PSD analysis provides information of how the variance of the power signal as a function of frequency is distributed. Two different types of approach can be applied: parametric and non-parametric. The results of these approaches are similar and non-parametric approach is computationally simpler.

The non-parametric PSD estimation is based on Fast Fourier Transform (FFT). The result of such computation is the power spectrum from which LF and HF components will be extrapolated as described in the following sections.

2.7.3 Nonlinear methods

Nonlinear methods are based on chaos theory and fractal analysis. They allow to describe the heart complexity and the irregular fluctuations of HR. Therefore, nonlinear methods are applied to understand the HRV nonlinear phenomena.

A technique very popular in the scientific community is the Poincaré plot (*Figure 2.22*).

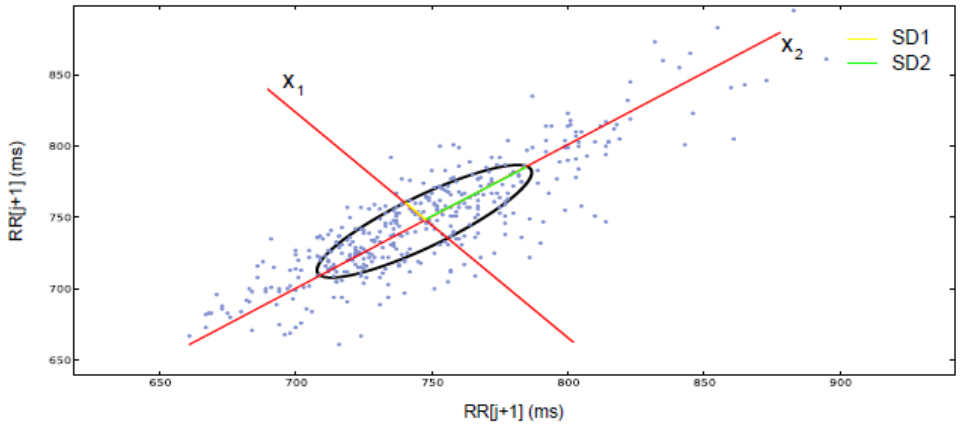

Figure 2.22: Poincaré plot analysis

2.8 Drowsiness detection using HRV

As previously discussed, the autonomic nervous system (ANS) activity can be estimated from the HRV signal. More specifically, the HRV signal presents a different behaviour during stressful, tiring situations and drowsiness episodes.

Thus, these HRV alterations are useful to evaluate autonomic activity and detect driver's drowsiness.
HRV changes during different sleep stages, showing a predominant parasymphatetic activity during non-rapid eye movement sleep and an increased sympathetic activity during rapid eye movement sleep.

This difference is more evident considering the following *Figure 2.23*, where the PPG signal pattern of awake (*Figure 2.23.a*) and drowsy (*Figure 2.23.b*) states is represented. Awake state waveforms have narrow intervals and high amplitude, whereas drowsy state waveforms are characterized by broader intervals and lower amplitudes.

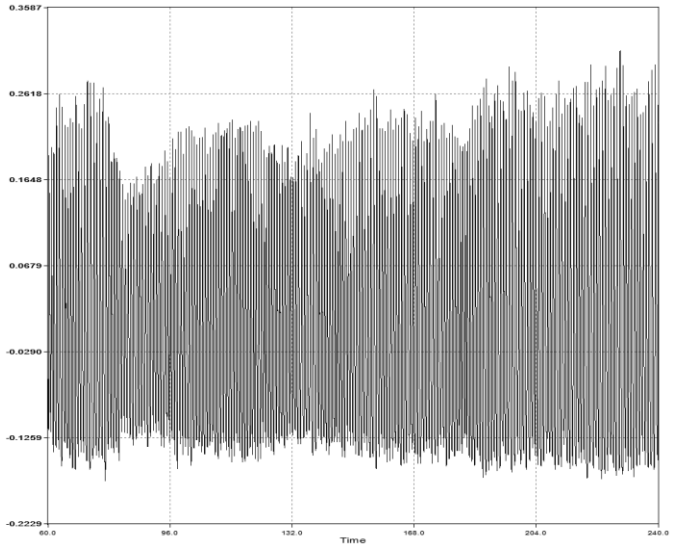

(a)

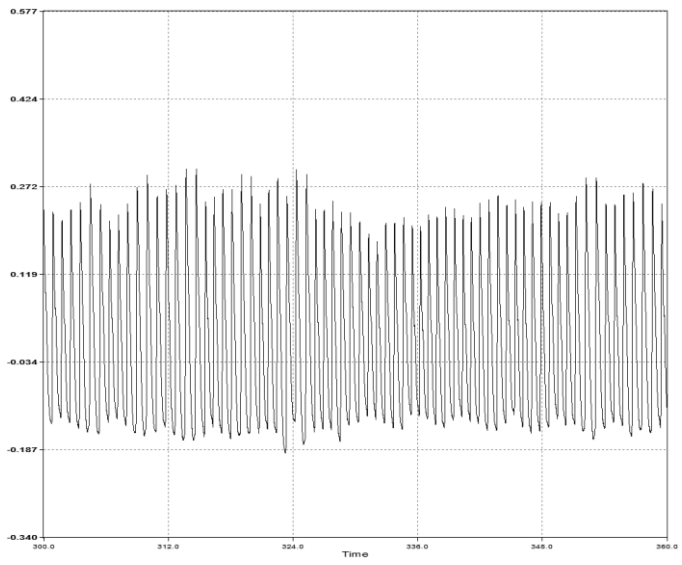

(b)

Figure 2.23: PPG signal of awake (a) and drowsy state (b)

Kim et al. [57] analysed the HRV signals in the time and in the frequency domain. The result of this study indicated a significant decrease in the heart rate (in the time domain) with the R-R interval of ECG faster in case of driver in drowsy state [4].

As already stated, the HRV signal can be obtained from ECG or PPG. Several studies analysed the HRV-drowsiness state correlation. Drowsy driving could be detected using the Low Frequency (LF), the High Frequency (HF) measures and them ratio LF/HF value of HRV signal. These measures are derived from the spectral analysis of the R-R intervals [13]. *Figure 2.24* represents the LF and HF derivations. Firstly, some stable R-R intervals of the ECG signal is chosen. Then, through a spectral analysis of different R-R intervals, LF and HF are extrapolated from the power spectrum.

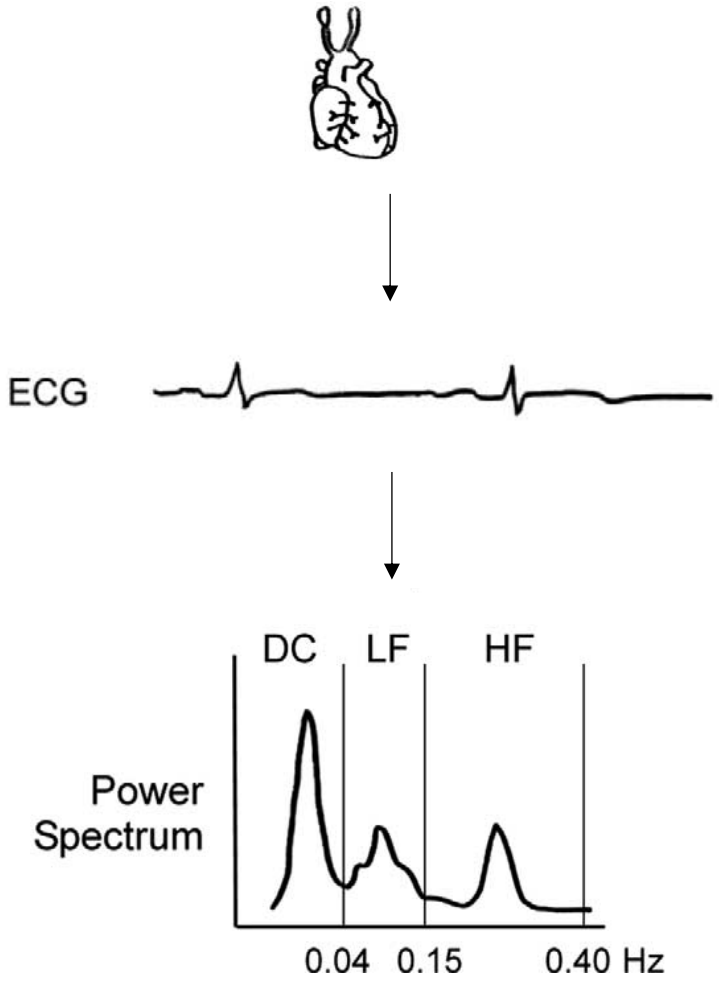

Figure 2.24: LF and HF derivation (figure modified from [13])

The spectral analysis produces a power spectrum ranging from 0 to 0.4 Hz.

LF and HF intervals are in the 0.04-0.15 Hz and 0.15-0.4 Hz, respectively [71], [4].
These specific frequency intervals are a marker of sympathetic and parasympathetic nervous activities. More precisely, HF is a measure of cardiac parasympathetic activity in humans. LF is considered to reflect both sympathetic and parasympathetic activities even if is not a specific measure of cardiac sympathetic activity. Despite this, since LF is easily calculated, it is considered as a marker of cardiac sympathetic activity. Their ratio LF/HF is considered as an index of the sympathovagal balance [13].

Certain studies [4] established the connection between these frequency intervals, their ratio LF/HF and drowsy driving condition. The outcome of this research is summarised by the following *Table 2*:

	Standard	Example	Example	Example
LF	decrease	increase	decrease	increase
HF	increase	increase	decrease	decrease
LF/HF	decrease	increase	decrease	increase
Decision	drowsy	awake	awake	awake

Table 2.2: Drowsy decision criteria [4]

Thus, during drowsy driving LF decreases and HF increases, resulting in decreased LF/HF ratio (*Figure 2.25.b*). Awake driving is characterized by three different scenarios: increased LF, HF, and LF/HF values; decreased LF, HF, and LF/HF values; and, finally, increased LF, decreased HF and increased LF/HF ratio (*Figure 2.25.a*) [4].

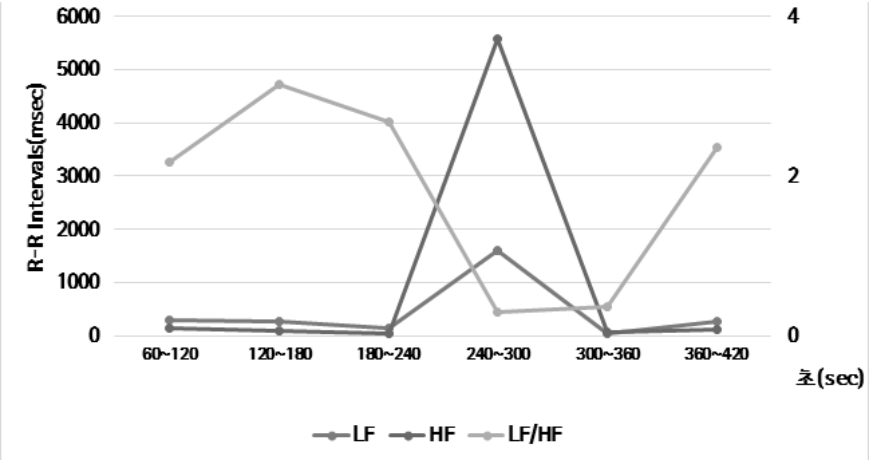

(a)

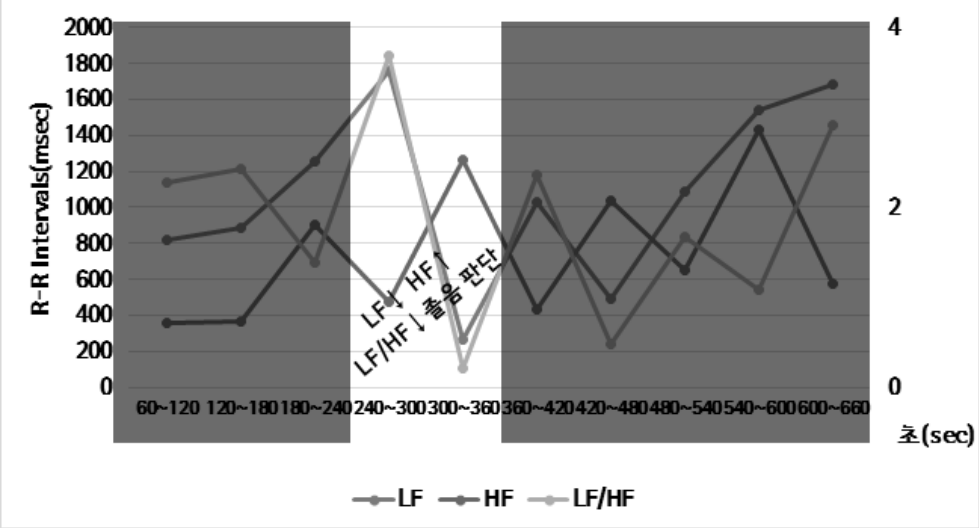

(b)

Figure 2.25: LF, HF, LF/HF trends for awake (a) and drowsy state (b) [4]

Another study [3] considers only HF and LF/HF values as indices of the autonomous nerve activity. In particular, HF indicates the parasympathetic nervous activity, whereas LF/HF indicates the sympathetic nervous activity. According to this study, during the drowsiness state, LF increases by 57.1% at the moment of drowsiness onset and HF increases by 49.2% during drowsy state (*Figure 2.26*).
Furthermore, as it can be seen in the following *Figure 2.27*, LF/HF increases by 105%.

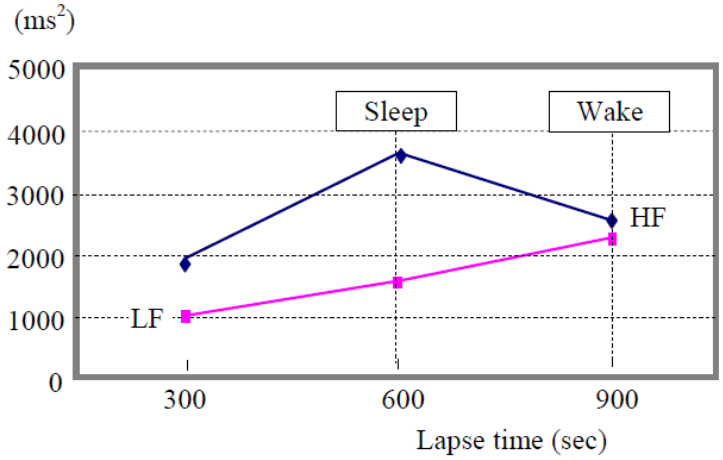

Figure 2.26: LF, HF trends for awake and drowsy state [4]

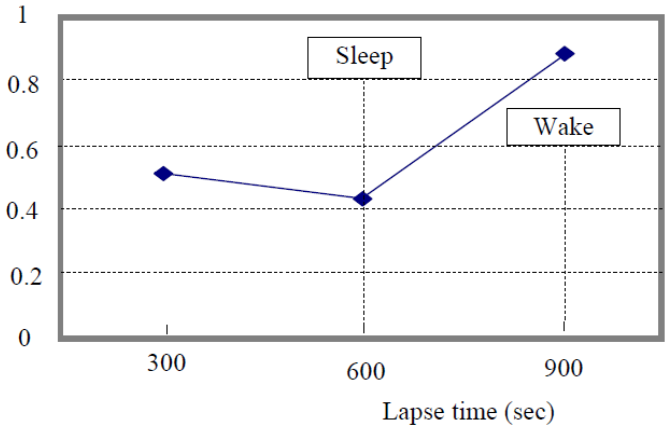

Figure 2.27: LF/ HF trends for awake and drowsy state [4]

2.9 Polysomnography

Polysomnography is a multi-parametric and a non-invasive test used to study sleep activity and diagnose sleep disorders. The test result is referred to as polysomnogram (PSG) and it is performed while patient is asleep, typically during the night.

This test aims at investigating symptoms that may cause sleep disorders as:

- sleep apnoea
- periodic limb movement disorder
- narcolepsy
- REM sleep behaviour disorder
- chronic insomnia

The PSG is performed in a controlled environment and monitored by qualified polysomnography professionals. Before a PSG, patients are invited to avoid the consumption of alcohol and caffeine, which may affect the test result.

A standard polysomnogram procedure starts in the late evening. The first 1-2 hours are spent putting all the electrodes and channels in the required place. Typically, the number of channels of data to efficiently carry out the test is 12. A sleep technician is responsible for attaching the electrodes and monitoring the patient during the test.

Different body functions are monitored during the PPG:

- the eye movements, detected through the electrooculogram EOG
- the brain waves, recorded with the electroencephalogram EEG

- the heart rhythm, measured through the electrocardiogram ECG
- skeletal muscle activation, recorded through the electromyogram EMG
- the breathing rate, measured using a peripheral pulse oximetry
- sounds made while sleeping, through a sound probe.

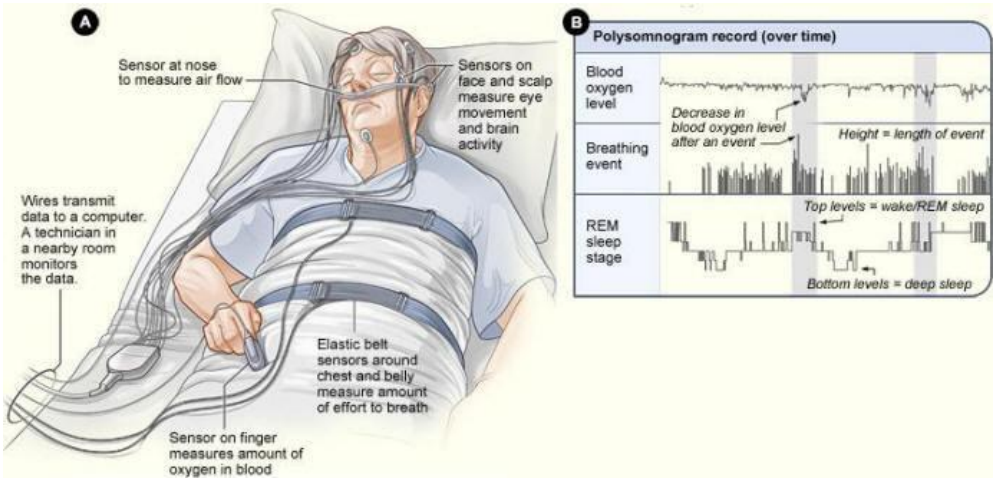

Figure 2.28: PSG test

A minimum of three channels are used for the **electroencephalogram** (EEG). Typically, six "exploring" and two "reference" electrodes are used. The "exploring" electrodes are placed on the scalp near the frontal, central, and occipital portions of the brain through a conductive paste. These electrodes provide a readout of the brain activity which corresponds to the REM, NREM and wakefulness stages.

For **the electrooculogram** (EOG) two electrodes are placed in correspondence of the outer canthus of the right and left eyes. These electrodes aim at determining the REM phase, characterized by rapid eye movements. Eye activity is detected through the electropotential difference between the cornea (more positively charged) and the retina.

The **electromyogram** (EMG) uses four electrodes. Its purpose is to measure muscle activity. Muscle tension and leg movements are monitored through four leads. Two leads are placed on the chin to detect the reduction in muscle tension typical of the REM phase. Two other leads are placed on the anterior tibial of each leg to measure leg movements.

Two or three electrodes are used for the **electrocardiogram** (ECG) and are positioned at the collarbone. The aim is to monitor cardiac activity in terms of contractions and expansions by recording the P wave, QRS complex and T wave.

The respiration rate and any interruptions in breathing are measured using pressure transducers and/or a thermocouple placed near the nostrils. Nasal and

oral airflow is observed using belts. Contraction and expansion of the belts indicate respiratory effort.

Sleep apnoea and other respiratory problems are related to changes in blood oxygen levels. A pulse oximeter is placed over a fingertip or an earlobe to detect changes in blood oxygen levels.

Snoring could be recorded through a sound probe over the neck.

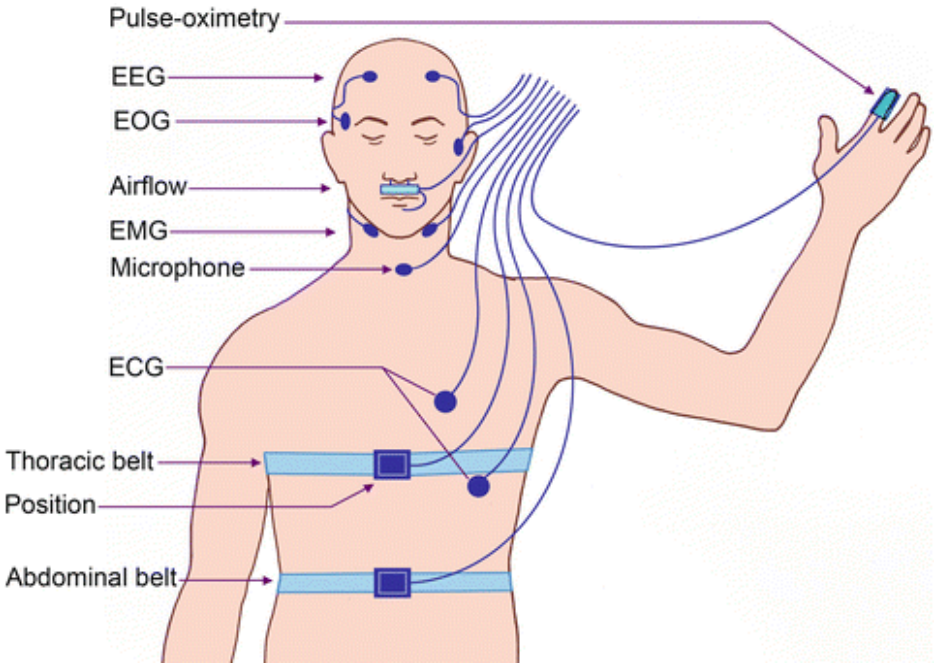

Figure 2.29: PSG test setup

The monitored body functions are recorded, and the collected data are used to create a graph. The resulting picture is an indicator of the overall sleep stages and quality (*Figure 2.30*) [15], [16], [17].

Figure 2.30: Typical polysomnogram tracing from [15]

Chapter 3

Driver drowsiness dataset

The data required to develop this work were collected using the AVL dynamic driving simulator, in Graz.
Participants were sleep deprived to make them more prone to drowsiness. For the measurement, all the subjects were equipped with PSG and they followed a pre-defined driving route. The driving task consisted of a city night path for the first 5-10 minutes, and then a straight highway path.
PSG signals were analysed by the sleep experts to build the ground truth for the sleep detection.
PPG signal was acquired, and the spectral analysis was performed.
These data have also been processed using a PPG-based sleep prediction algorithm able to predict the falling asleep of all the subjects based on HRV signal analysis [18].

Chapter 4

Methodology

4.1 System identification

4.1.1 Set-membership identification theory

Set-membership identification theory is a tool for deriving a parametric mathematical model of a plant. This model is derived from a set of input-output collected data and some a-priori information on the system.
The system to be identified can be:

- *static* (the output at time t_0 depends only on the input value at time t_0)
- *dynamic* (the output at time t_0 depends on the input at time t_0 and on the past inputs)

4.1.2 Set-membership identification a-priori information

Set-membership identification theory is based on the following three main pieces of information.

I. A-priori information on the system

The system is defined by a function by a function "f" describing the input-output mapping.

$$w(k) = f(\theta, r(k)) \tag{4.1}$$

where:

- θ is the parameter to be identified
- $r(k)$ is the regressor. It depends on the past values of the input and the output and (possibly) on the input at time k
- $f \in F$ and F is a model class (i.e., a given class function) to be known a-priori

For example, a reasonable assumption is to consider the system a linear time-invariant.

A linear time-invariant (LTI) system is a system characterized by an input-output relation subject to linearity and time-invariance properties. Therefore, due to the linearity property, the input-output relationship is a linear mapping. The time-invariance property implies that the output does not depend on the time at which the input is applied (*Figure 4.1*).

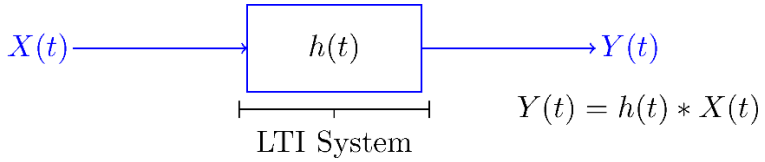

Figure 4.1: LTI system

For instance, the input-output relationship can be described as follows:

$$w(t) = -\alpha_1 w(t-1) - \cdots - \alpha_n w(t-n) + \beta_0 u(t) + \cdots + \beta_m u(t-m) \quad \forall t = 1, \ldots, N \tag{4.2}$$

where:

- $\alpha_1 \ldots \alpha_n$ and $\beta_0 \ldots \beta_m$ are the system parameters to be identified.

Consequently, the plant can be described by a discrete time transfer function:

$$G(q^{-1}) = \frac{\beta_0 + \beta_1 q^{-1} + \cdots + \beta_m q^{-m}}{1 + \alpha_1 q^{-1} + \cdots + \alpha_n q^{-n}} \tag{4.3}$$

II. A-priori information on the noise affecting the collected data

The a-priori information on the noise is related to the noise amplitude bounds and to the noise model structure.
The noise affecting the data $e(t)$ is assumed to belong to a given bounded set Δe:

$$|e(t)| \leq \Delta e, \qquad \forall t = 1, \ldots, N \tag{4.4}$$

Noise model structure refers to the way the noise affecting the collected experimental data enters the problem. There are three main topologies:

- ***Equation Error (EE) structure***
  In the EE structure, the collected output sequence is corrupted by a noise given by applying a signal e(t) through a filter with a numerator equal to 1 and the same denominator of the system plant (*Figure 4.2*).

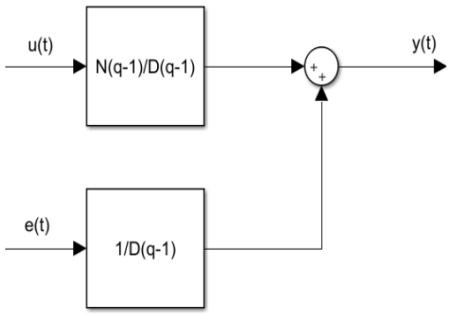

Figure 4.2: EE model structure from [19]

- ***Output Error (OE) structure***
  In the OE structure, the collected output sequence is corrupted by a random noise (*Figure 4.3*). This situation typically occurs when the input signal is provided and the output signal is collected by means of a measurement device.

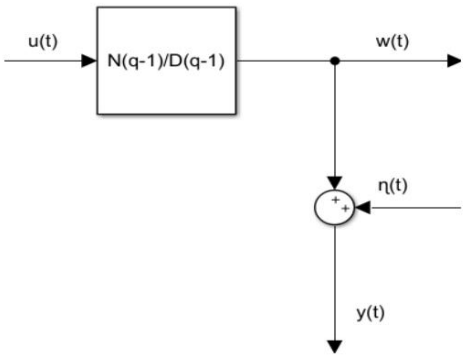

Figure 4.3: OE structure from [19]

For example, considering a LTI system:

$$y(t) = w(t) + \eta(t)$$

$$w(t) = -\alpha_1 w(t-1) - \cdots - \alpha_n w(t-n) + \beta_0 u(t) + \cdots + \beta_m u(t-m)$$

$$\Downarrow$$

$$y(t) - \eta(t) = -\alpha_1 y(t-1) + \alpha_1 \eta(t-1) - \cdots - \alpha_n y(t-n) + \\ + \alpha_n \eta(t-n) + \beta_0 u(t) + \cdots + \beta_m u(t-m)$$

where:

- $u(t)$ is the true input applied to the system
- $w(t)$ is the true output
- $\eta(t)$ is the output measurement error
- $y(t)$ is the true measured output (affected by noise)

- ***Errors-In-Variables (EIV) structure***
  In the EIV structure, both the input and the output are corrupted by uncertainties (*Figure 4.4*).
  This situation typically occurs when the input and the output are experimentally collected.
  The input error ε(t) and the output error η(t) are considered as variables with unknown behaviour belonging to a given bounded set:

$$|\varepsilon(t)| \leq \Delta\varepsilon, \qquad \forall t = 1, \dots, N$$
$$|\eta(t)| \leq \Delta\eta, \qquad \forall t = 1, \dots, N$$
$\triangle\ \varepsilon, \triangle\ \eta$ are known bounds.

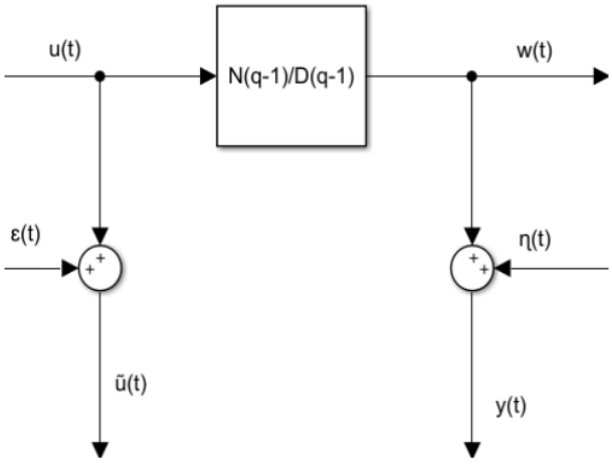

Figure 4.4: EIV structure from [19]

For example, considering a LTI system:

$$\tilde{u}(t) = u(t) + \varepsilon(t)$$
$$y(t) = w(t) + \eta(t)$$

$$w(t) = -\alpha_1 w(t-1) - \cdots - \alpha_n w(t-n) + \beta_0 u(t) + \cdots + \beta_m u(t-m)$$

$$\Downarrow$$

$$y(t) - \eta(t) = -\alpha_1 y(t-1) + \alpha_1 \eta(t-1) - \cdots - \alpha_n y(t-n) + \\ + \alpha_n \eta(t-n) + \beta_0 \tilde{u}(t) - \beta_0 \varepsilon(t) + \cdots + \beta_m \tilde{u}(t-m) - \beta_m \varepsilon(t-m)$$

where:

- $u(t)$ is the true input applied to the system
- $w(t)$ is the true output
- $\varepsilon(t)$ is the input measurement error
- $\eta(t)$ is the output measurement error
- $\tilde{u}(t)$ is the measured input (affected by noise)
- $y(t)$ is the measured output (affected by noise)

III. <u>A set of input-output collected data</u>

The input-output data are experimentally collected on the real system. These data are affected by noise due to their inherent experimental nature.

4.1.3 Polynomial optimization problem for the PUIs computation

In set-membership estimation theory, the ***feasible solution set*** (FSS) is the set of all the models that are consistent with:

i. the available a-priori information on the system
ii. the available a-priori information on the noise
iii. the collected input-output data

If the class of the system F is parametrized by a parameter vector θ, the FSS can be replaced by the ***feasible parameter set*** $\boldsymbol{D_\theta}$ (FPS). The FPS is the set of all the parameters θ_i that satisfies the equations describing the system for all the collected input-output data.

The ***extended feasible parameter set*** $\boldsymbol{D_{\theta,\eta,\varepsilon}}$ (EFPS) is the space of the system parameters θ_i and the error variables (in the case of EIV structure η and ε). The EFPS is a reformulation of the problem in a higher space variable.

For example, considering the EIV structure, the EFPS is defined as follows.

$$
\begin{aligned}
D_{\theta,\eta,\varepsilon} = \{\theta \in \Re^{2n+1},\ \eta \in \Re^N,\ \varepsilon \in \Re^N:\\
y(t) - \eta(t) = -\theta_1 y(t-1) + \theta_1 \eta(t-1) + \cdots + \theta_{2n+1}\tilde{u}(t-n)\\
- \theta_{2n+1}\varepsilon(t-n) \qquad \forall t = n+1, \ldots, N\\
|\varepsilon(t)| \le \Delta\varepsilon, \qquad \forall t = 1, \ldots, N\\
|\eta(t)| \le \Delta\eta, \qquad \forall t = 1, \ldots, N\ \}
\end{aligned}
$$

The ***parameter uncertainty intervals*** (PUIs) are the extreme values (minimum and maximum values) of the parameters θ_i. For instance, in the EIV problem:

$$
PUI_{\theta_j} = [\underline{\theta_j}, \overline{\theta_j}]
$$

$$
\begin{aligned}
subject\ to\\
y(t) - \eta(t) = -\theta_1 y(t-1) + \theta_1 \eta(t-1) + \cdots + \theta_{2n+1}\tilde{u}(t-n)\\
- \theta_{2n+1}\varepsilon(t-n) \qquad \forall t = n+1, \ldots, N\\
|\varepsilon(t)| \le \Delta\varepsilon, \qquad \forall t = 1, \ldots, N\\
|\eta(t)| \le \Delta\eta, \qquad \forall t = 1, \ldots, N
\end{aligned}
$$

where:

- $\underline{\theta_j} = min\,\theta_j$
- $\overline{\theta_j} = max\theta_j$
- $\theta_j \in D_{\theta,\eta,\varepsilon}$
- N is the number of collected data

For example, considering the two-dimensional problem in *Figure 4.5*, the PUIs of θ_1 are $\underline{\theta_1}$ (minimum value) and $\overline{\theta_1}$ (maximum value).

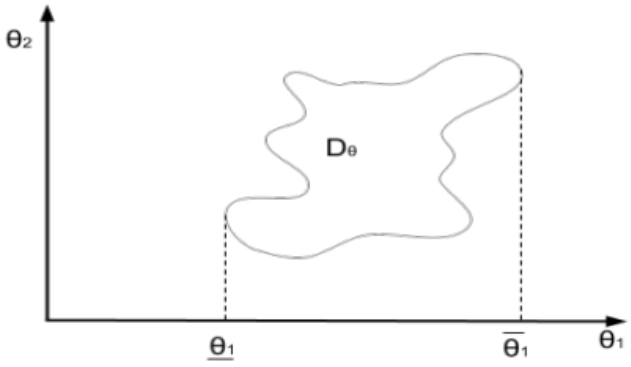

Figure 4.5: PUI of θ_l from [19]

The FPS and the EFPS have a complex shape, difficult to be handled mathematically. PUIs computation is preferable since it is simpler and consists of an outrebounding approximation on the FPS or the EFPS.
The PUIs computation requires to compute the global optima solution of the following optimization problems:

1) $\underline{\theta_j} = min\,\theta_j \qquad \forall j = 1, \dots, 2n+1$

2) $\overline{\theta_j} = max\theta_j \qquad \forall j = 1, \dots, 2n+1$

As it can be noticed, the following terms in bold are nonlinear terms (more specifically, bilinear). Therefore, the problem under consideration is a polynomial optimization problem (POPs).

$$PUI_{\theta_j} = [\underline{\theta_j}\,, \overline{\theta_j}\,]$$

$$subject\ to$$

$$y(t) - \eta(t) = -\theta_1 y(t-1) + \theta_1 \eta(t-1) + \cdots + \theta_{2n+1}\tilde{u}(t-n) - \theta_{2n+1}\varepsilon(t-n) \qquad \forall t = n+1, \dots, N$$

$$|\varepsilon(t)| \le \Delta\varepsilon, \qquad \forall t = 1, \dots, N$$

$$|\eta(t)| \le \Delta\eta, \qquad \forall t = 1, \dots, N$$

Typically, POPs are nonlinear and nonconvex optimization problems. Due to nonconvex property, POPs could have some local minimum solutions and "standard" mathematical tools can trap into local minima.
Convex relaxation approach is a tool for the computation of global optimal solution of a POPs problem. This method allows to compute a convex relaxation of the FPS. In particular, the nonconvex FPS is approximated by a convex set including the original FPS (*Figure 4.6*).

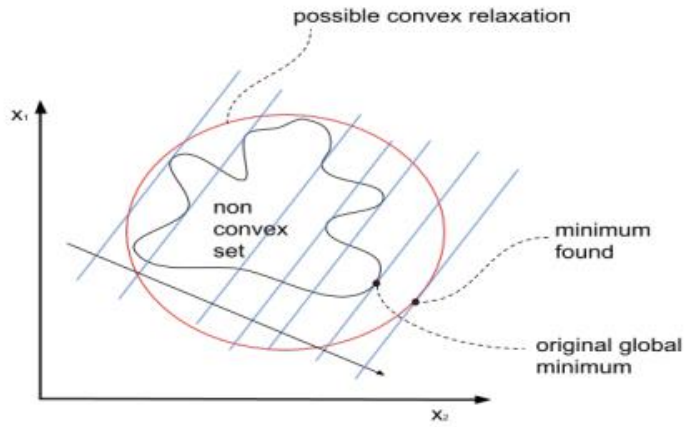

Figure 4.6: Convex relaxation approximation from [19]

Convex relaxation solution depends on a parameter referred as ***order of relaxation δ***:

- when $\delta \to \infty$,the convex approximation tends to the convex hull (i.e., the smallest convex set covering the original nonconvex set) of the FPS (*Figure 4.7*)

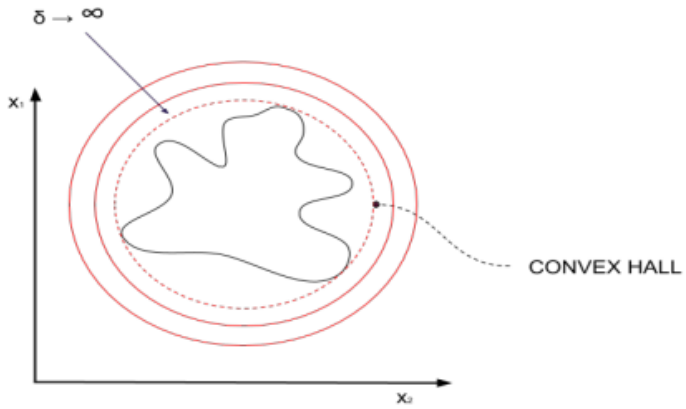

Figure 4.7: Convex hull from [19]

- computational complexity grows as δ increases
- δ_{MIN} is the minimum possible order of relaxation that can be considered for applying convex relaxation techniques

$$\delta_{MIN} = \left\lfloor \frac{\max\ \_degree}{2} \right\rfloor \tag{4.5}$$

where:

- max $\_degree$ is the higher degree of the polynomial constraints
- ⌊x⌋ is the ceiling operator

For this thesis work, SparsePOP Matlab package has been used for finding global optimal solution of POPs. The solver used for approximating the global optimal solution was SeDuMi.

4.1.3 Set-membership identification for drowsiness detection application

For this work, the implementation of two system transfer functions have been considered:

- the SISO transfer function $G_1(z)$ between dmRR (differential of the medium value of the respiration rate, as input) and dHF (differential value of HF, as output)
- the SISO transfer function $G_2(z)$ between dsRR (differential of the standard deviation, as input) and dlambda (differential value of lambda, as output)

The mathematical model of the plant has been identified on the basis of the following informations.

I. <u>A-priori information on the system</u>

In both the cases, the system has been assumed to be a LTI system of order $n = 2$.
Therefore, the system transfer functions are described by the following equation:

$$G(q^{-1}) = \frac{\theta_3 + \theta_4 q^{-1} + \theta_5 q^{-2}}{1 + \theta_1 q^{-1} + \theta_2 q^{-2}} \tag{4.6}$$

II. <u>A-priori information on the noise</u>

The noise is assumed to enter the system as an EIV:

$$\begin{aligned} \tilde{u}(t) &= u(t) + \varepsilon(t) \\ y(t) &= w(t) + \eta(t) \\ |\varepsilon(t)| &\leq 1, \qquad \forall t = 1, \dots, N \\ |\eta(t)| &\leq 1, \qquad \forall t = 1, \dots, N \end{aligned}$$

Noise bounds $\Delta\varepsilon$ and $\Delta\eta$ are assumed to be equal to 1.

III. A set of input-output collected data

A set of data has been collected through the PSG test and the power spectrum analysis of the PPG signal.

For the computation of $G_1(z)$, the following data have been considered:

- *INPUT*: the differential of the medium value of the respiration rate (dmRR), from the PSG test.
- *OUTPUT*: the differential value of HF (dHF), from the power spectrum analysis.

Both the input and the output have been calculated by examining sliding windows of 2048 samples.

For the computation of $G_2(z)$, the following data have been considered:

- *INPUT*: differential of the standard deviation, as input (dsRR), from the PSG test.
- *OUTPUT*: the differential value of lambda (dlambda), from the power spectrum analysis.

Also in this case, the input and the output have been calculated by examining sliding windows of 2048 samples.

4.1.4 Computation of the PUIs

PUIs has been computed by solving the following optimization problems:

1)

$$\underline{\theta_j} = \min \theta_j$$

$$subject\ to$$

$$\begin{aligned} y(t) - \eta(t) = &-\theta_1 y(t-1) + \theta_1 \eta(t-1) - \theta_2 y(t-2) + \theta_2 \eta(t-2) + \theta_3 \tilde{u}(t) \\ &+ \cdots - \theta_3 \varepsilon(t) + \theta_4 \tilde{u}(t-1) - \theta_4 \varepsilon(t-1) + \theta_5 \tilde{u}(t-2) \\ &- \theta_5 \varepsilon(t-2) \end{aligned}$$

$$\forall t = n+1, \dots, N$$

$$|\varepsilon(t)| \leq 1, \qquad \forall t = 1, \dots, N$$

$$|\eta(t)| \leq 1, \qquad \forall t = 1, \dots, N$$

2)

$$\overline{\theta_j} = \max \theta_j = \min(-\theta_j)$$

$$subject\ to$$

$$\begin{aligned} y(t) - \eta(t) = & -\theta_1 y(t-1) + \theta_1 \eta(t-1) - \theta_2 y(t-2) + \theta_2 \eta(t-2) + \theta_3 \tilde{u}(t) \\ & + \cdots - \theta_3 \varepsilon(t) + \theta_4 \tilde{u}(t-1) - \theta_4 \varepsilon(t-1) + \theta_5 \tilde{u}(t-2) \\ & - \theta_5 \varepsilon(t-2) \end{aligned}$$

$$\forall t = n+1, \dots, N$$

$$|\varepsilon(t)| \leq 1, \qquad \forall t = 1, \dots, N$$

$$|\eta(t)| \leq 1, \qquad \forall t = 1, \dots, N$$

$$\Downarrow$$

$$PUI_{\theta_j} = [\underline{\theta_j}, \overline{\theta_j}]$$

This problem has been solved on Matlab through SparsePOP package.

The chosen relaxation order for this computation was the minimum possible: $\delta = 1$.
Finally, the Chebychev centre θ_j^C of the EFPS has been computed to find the central estimate of each parameter θ_j :

$$\theta_j^C = \frac{\underline{\theta_j} + \overline{\theta_j}}{2} \tag{4.7}$$

The resulting transfer functions have been reformulated in state space form to be implemented in the drowsiness detection algorithm.

4.2. Respiration Rate-based algorithms for drowsiness detection

The aim of this thesis is to develop an algorithm able to detect signs of sleepiness in drivers.

Two very similar algorithms have been developed and compared. The real-time algorithms have been developed considering the ANS activity correlation with some parameters (more specifically, dHF and dlambda) from the spectral analysis

of the PPG signal. Indeed, ANS activity is strictly related to the state of driver, as previously mentioned.

The future application will be the implementation on a contactless device, e.g. a short-range radar. The operation of short-range radar is based on the electromagnetic backscattering phenomena. The backscattering is the reflection of waves, particles, signals back to the original direction.
This technology is implemented in healthcare application for detecting physiological movements due to heartbeat and respiration without using any sensor attached to the human body. Indeed, they are referred to as "short range" since the distance between the radar the target is of few meters or less.

Nevertheless, the PPG signal is not readily available on these devices. These devices allow to measure some biometrical parameters such as the respiration rate (RR).
Therefore, it was necessary to find a link between these biometrical parameters and the spectral analysis parameters from the PPG signal (and then to the activity of ANS).
The link between the RR and PPG signals has been found through the set-membership identification theory analysed in the previous chapter.
More specifically:

I. in the first algorithm (***A1***), drowsy driving has been detected through a calibration parameter related to the differential value of lambda (dlambda). An estimation of dlambda has been calculated starting from dsRR (differential value of the standard deviation of the RR values within a certain window).

II. in the second algorithm (***A2***), drowsy driving has been detected through a calibration parameter related to the differential value of the high frequency component of the PPG signal (dHF).
An estimation of dHF has been calculated starting from dmRR (differential value of the avarage of the RR values within a certain window).

The algorithms have been developed on Matlab.

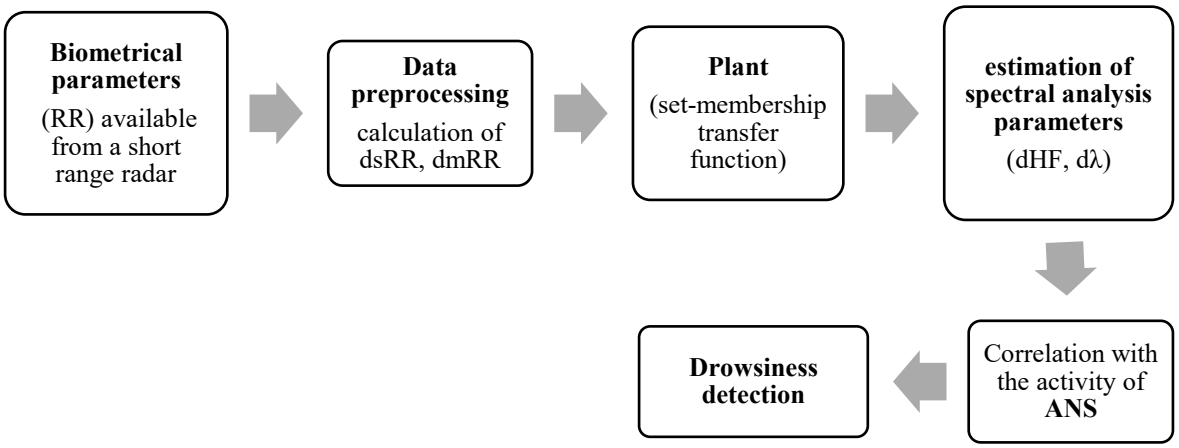

Figure 4.8: Summary diagram of the sleep detection algorithm

4.2.1. Development of the algorithms

As mentioned above, different datasets have been analysed to validate the algorithms. The data from the PSG analysis and the PPG signal were organised in Excel files. From these Excel files, some information relevant to the algorithm have been selected:

- the ***PPG signal***, acquired with a frequency of 50 Hz. Its power spectral analysis has been examined
- the ***RR signal*** from PSG analysis
- the ***state of the driver***, analysed by the sleep experts to build the ground truth for the sleep detection. In particular, the state has been identified as:

$$\begin{cases} \mathbf{0}, & if\ the\ state\ is\ unsure \\ \mathbf{1}, & if\ the\ state\ is\ sleep \\ \mathbf{-1}, & if\ the\ state\ is\ awake \end{cases}$$

For the analysis of the data, jumping windows of 2048 data have been considered.

The spectral analysis of the PPG signal in each window is performed. This allows the maximum of the low frequency (LF) and high frequency (HF) contributions of the PPG signal to be calculated. As mentioned before, the ratio of these two

contributions is related to ANS activity and to the possible scenario of drowsy driving.

Therefore, the ratio λ is calculated in each window:

$$\lambda = \frac{LF}{HF} \tag{4.8}$$

where:

- LF is the maximum of low frequency contributions in the 0.04-0.15 Hz interval
- HF is the maximum of high frequency contributions in the 0.15-0.4 Hz interval

This information is in common and used in the development of both the algorithms. The differences between them consist of:

- the biometric contribution as input (dsRR or dmRR) and the spectral variable as output ($d\lambda$ and dHF, respectively)
- the state matrices A, B, C, D from the set-membership identification
- the considered calibration parameters $d\lambda_{LIM}$ and dHF_{LIM}

The respiration rate (RR) from PSG analysis has been chosen as parameter to be filtered to obtain a relationship with the contributions of the power spectrum of the PPG signal.

Within each window, for the first algorithm A1, the standard deviation of the RR values (sRR) has been calculated.

The $dsRR$ (differential value of sRR) has been calculated as the absolute difference between the value of sRR in the current window i and the value of sRR assumed in the previous window $i-1$.

$$dsRR(i) = |sRR(i) - sRR(i-1)| \tag{4.9}$$

In each window *i*, the predicted value of $d\lambda$ (differential value of λ) has been computed through the transfer function calculated with the set-membership identification theory. This transfer function has been converted into state space representation form, obtaining the A, B, C, D matrices for the $d\lambda$ computation:

$$\begin{cases} \dot{x} = Ax + BdsRR \\ d\lambda = Cx + DdsRR \end{cases}$$

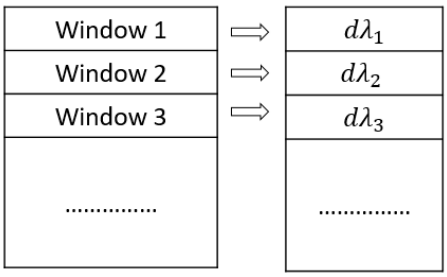

Figure 4.9: Computation of $d\lambda$ in each window

The initial state x has been considered as a zero-state vector.

The calibration parameter $d\lambda_{LIM}$ has been calculated considering the values assumed by $d\lambda$ in the first N windows. More specifically, it has been calculated as a linear function of the maximum value assumed by $d\lambda$ in these N windows:

$$d\lambda_{LIM} = \alpha \times \max(d\lambda) \tag{4.10}$$

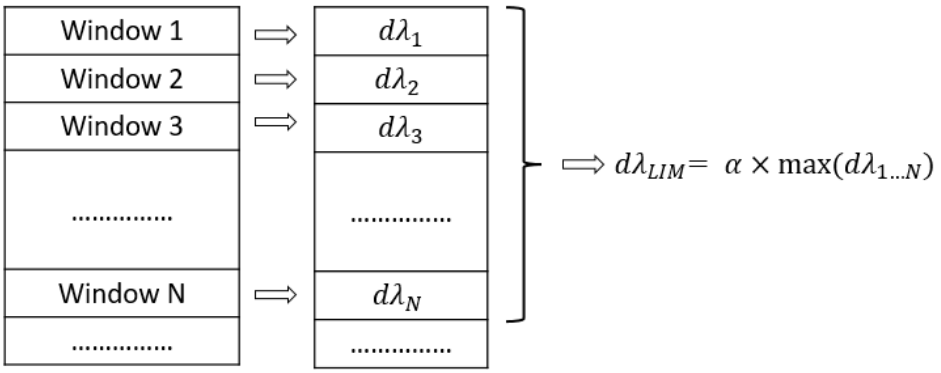

Figure 4.10: Computation of $d\lambda_{LIM}$

The successive values taken by $d\lambda$, compared with the calibration parameter $d\lambda_{LIM}$, has been considered as index of the driver's state. More specifically, the values assumed by $d\lambda$ have been analysed considering a set of N' of observation windows. Within this number of windows, if more than a certain number N'' of dHF values is lower than the $d\lambda_{LIM}$ calibration value, the subject has been considered to be drowsy.

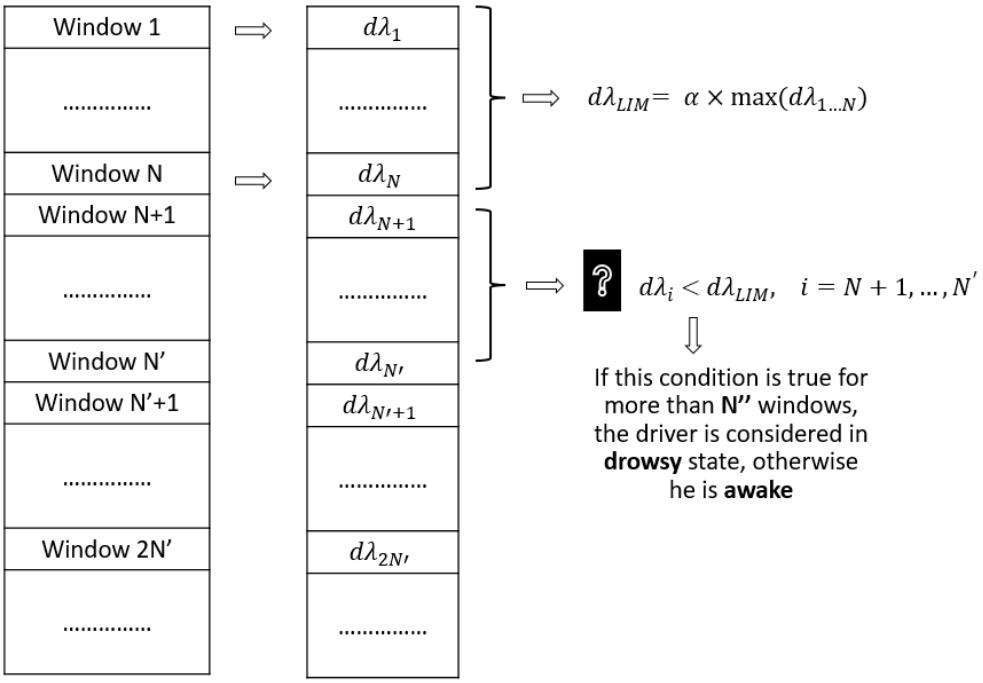

Figure 4.11: Comparison of $d\lambda_{LIM}$ - $d\lambda$ values on a set of windows

Within each window, for the second algorithm A2, the average of the RR values (mRR) has been calculated in each window.

The $dmRR$ (differential value of mRR) has been computed as the absolute difference between the value of mRR in the current window i and the value of mRR assumed in the previous window $i-1$.

$$dmRR(i) = |mRR(i) - mRR(i-1)| \tag{4.11}$$

In each window i, the predicted value of dHF (differential value of the high frequency contribution) has been calculated through the transfer function calculated with the set-membership identification theory. This transfer function has been converted into state space representation form, obtaining the A, B, C, D matrices for the dHF computation:

$$\begin{cases} \dot{x} = Ax + BdmRR \\ dHF = Cx + DdmRR \end{cases}$$

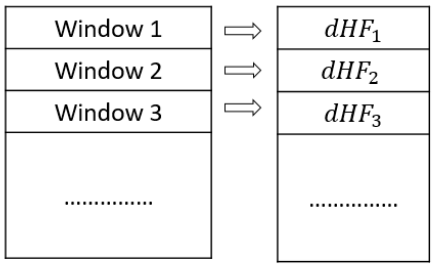

Figure 4.12: Computation of dHF in each window

The initial state x has been considered as a zero-state vector.

The calibration parameter dHF_{LIM} has been calculated considering the values assumed by dHF in the first N windows. More specifically, it has been calculated as a linear function of the maximum value assumed by dHF in these N windows:

$$dHF_{LIM} = \alpha \times \max(dHF) \tag{4.12}$$

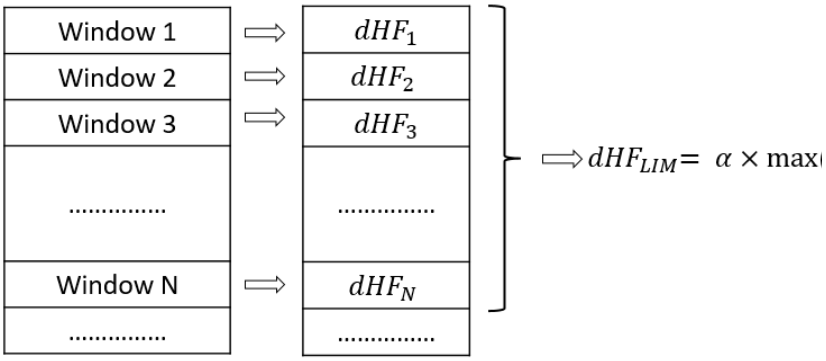

Figure 4.13: Computation of dHF_{LIM}

The successive values taken by dHF, compared with the calibration parameter dHF_{LIM}, has been considered as index of the driver's state. More specifically, the values assumed by dHF have been analysed considering a set of N' of observation windows. Within this number of windows, if more than a certain number N'' of

dHF values is lower than the dHF_{LIM} calibration value, the subject has been considered to be drowsy.

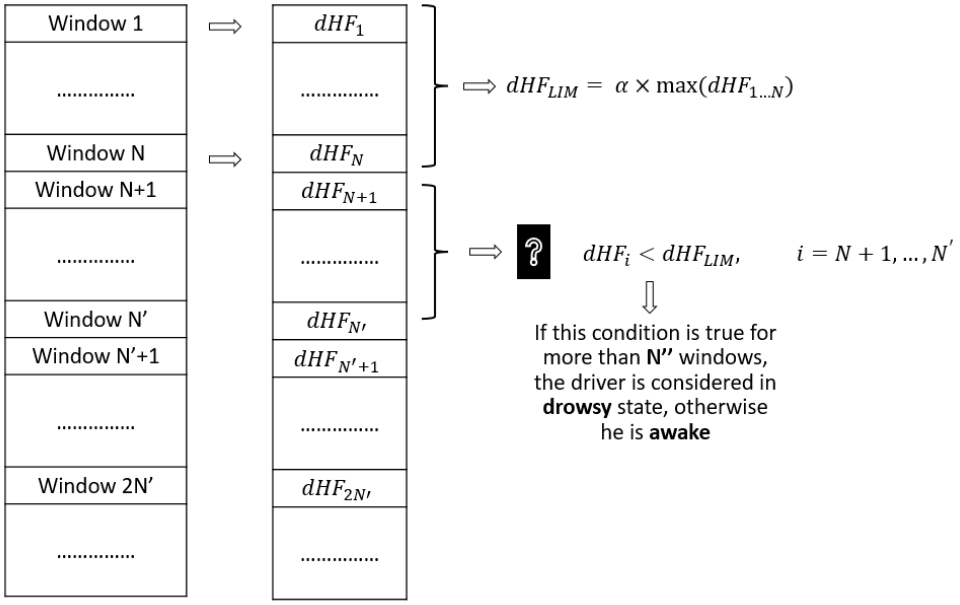

Figure 4.14: Comparison of dHF_{LIM} - dHF values on a set of windows

Chapter 5

Analysis of the results

The results obtained by applying this algorithm to different sets of data are shown in the following table:

Dataset	Sleep experts' sleep state detection (state = 1)	Sleep experts' unsure state detection (state = 0)	Algorithm 1 drowsiness detection	Algorithm 2 drowsiness detection
a	17:55:57	None	10:47:31	10:48:12
b	11:49:49	None	11:51:04	11:43:28
c	13:56:54	None	13:52:22	13:49:54
d	None	16:23:43	16:08:52	16:10:14
e	17:13:00	None	17:11:55	17:09:11
f	17:59:43	None	17:57:33	17:56:36

Table 5.1: Results of algorithm 1 and algorithm 2 in terms of sleep prediction time

This table shows:

- the falling asleep times noted by sleep medicine experts in the ground truth
- the predicted first falling asleep of the two algorithms

It can be noticed that the algorithms anticipate in most of the cases the falling asleep.

In the following, basic notions of sensitivity and specificity are given to better analyse the accuracy of the results of the algorithms.

Sensitivity or true positive rate (TPR) describes the algorithm capability to identify true positives:

$$TPR = \frac{TP}{P} = \frac{TP}{TP + FN} \tag{5.1}$$

where:

- P is the positive condition. It is the number of real positive conditions in the data. In this thesis work, P corresponds to the sleep state condition identified by sleep medicine experts: $state = 1$
- TP stands for true positive. It indicates an algorithm result describing properly the presence of a condition.
  In this case, TP occurs when the test result correctly indicates the sleep state condition.
- FN stands for false negative. It indicates an algorithm result describing wrongly the absence of a condition.
  In this case, FN occurs when the algorithm result wrongly indicates the awake and unsure state.

Specificity or true negative rate (TNR) describes the algorithm capability to identify true negatives.

$$TNR = \frac{TN}{N} = \frac{TN}{TN + FP} \tag{5.2}$$

where:

- N is the negative condition. It is the number of real negative conditions in the data. In this thesis work, N corresponds to the awake and unsure state conditions identified by sleep medicine experts: $state = -1$ and $state = 0$, respectively
- TN stands for true negative. It indicates an algorithm result that properly describe the absence of a condition.
  In this case, TN occurs when the algorithm result correctly indicates the awake and unsure state.
- FP indicates an algorithm result that wrongly describe the presence of a condition.
  In this case, FP occurs when the algorithm result wrongly indicates the sleep state.

The results of the two algorithms are shown in the following tables.

Dataset	Sleep experts' sleep state detection (state = 1)	Sleep experts' unsure state detection (state = 0)	Algorithm 1 drowsiness detection	Algorithm 1 results
a	17:55:57	None	10:47:31	TP-TN
b	11:49:49	None	11:51:04	FN
c	13:56:54	None	13:52:22	TP-TN
d	None	16:23:43	16:08:52	FP
e	17:13:00	None	17:11:55	TP-TN
f	17:59:43	None	17:57:33	TP-TN

Table 5.2: Results of algorithm 1

Dataset	Sleep experts' sleep state detection (state = 1)	Sleep experts' unsure state detection (state = 0)	Algorithm 2 drowsiness detection	Algorithm 2 results
a	17:55:57	None	10:48:12	TP-TN
b	11:49:49	None	11:43:28	TP-TN
c	13:56:54	None	13:49:54	TP-TN
d	None	16:23:43	16:10:14	FP
e	17:13:00	None	17:09:11	TP-TN
f	17:59:43	None	17:56:36	TP-TN

Table 5.3: Results of algorithm 2

The TN and TP results of the algorithms are related to the state of the driver until the first sleep. Thus, when the driver is awake and the algorithm indicates the awake state, the result is TN; when the driver falls asleep and the algorithm correctly indicates the sleep state, the result is TP. For this reason, TN and TP results are present in the same datasets.

Therefore, the resulting TPR_1 and TNR_1 (sensitivity and specificity of the algorithm 1) are:

$$TPR_1 = \frac{4}{4+1} = 0.8$$

$$TNR_1 = \frac{4}{4+1} = 0.8$$

Therefore, the resulting TPR_2 and TNR_2 (sensitivity and specificity of the algorithm 2) are:

$$TPR_2 = \frac{5}{5} = 1$$

$$TNR_2 = \frac{5}{5+1} = 0.8\overline{3}$$

As the entire dataset analysed is rather small, TPR and TNR values should be considered as a rough estimate. Therefore, the efficiency of the algorithm needs to be confirmed and deepened with further data.

The FP results of both algorithms are present for the dataset "d", characterized by a state equal to 0 at a certain time. This type of state is referred to as "ensure" because it is an ambiguous state (i.e., sleep and awake state have not been identified effectively). Therefore, an undefined state was identified instead of the sleep state.
Furthermore, as the dataset available is small, the presence of this single FP significantly reduces the TNR for both algorithms.

Finally, it can be seen that the second algorithm provides better results. This is due to the fact that the dHF values are in the same frequency range as the dmRR values. Therefore, the estimation of dHF is more accurate than the estimation of dλ. Consequently, the virtual sensor that allows to estimate dHF (and then the sleep state) is more accurate.

Chapter 6

Conclusions

The aim of this thesis work was the development of an algorithm able to detect the falling asleep from the respiration rate (RR) signal.

In this application, the RR signal has been obtained from the PSG analysis.

Two virtual sensors have been built to link this biometrical signal with some power spectrum parameters (λ, HF) strictly related to the Autonomous Nervous System (ANS) activity and, consequently, to the sleep and awake states.
The power spectrum parameters used for building the virtual sensors have been computed from the power spectrum analysis of the PPG signal.
In particular, the virtual sensors aim at estimating the power spectrum parameters dλ and dHF.
Subsequently, based on the operation of this sensors, dHF_{LIM} and $d\lambda_{LIM}$ (the calibration values of dHF and dλ) have been computed. dHF_{LIM} and $d\lambda_{LIM}$ have been employed to allow the identification of sleep state.
The algorithms anticipated the falling asleep in most of the cases. Nevertheless, the results of the algorithm which relates dmRR and dHF were slightly better since dmRR and dHF belong to the same frequency band. Consequently, the system identification and the virtual sensor were more precise. Therefore, this algorithm is more accurate.

As mentioned before, the RR dataset for this application has been obtained through the use of a thorax band during the PSG test. The future application of this algorithm will be to implement it on a short-range radar able to detect RR data.

Bibliography

[1] Jin L, Niu Q, Jiang Y, Xian H, Qin Y, Xu M. Driver Sleepiness Detection System Based on Eye Movements Variables. Advances in Mechanical Engineering. January 2013. doi:10.1155/2013/648431

[2] Vicente, J., Laguna, P., Bartra, A. *et al.* Drowsiness detection using heart rate variability. *Med Biol Eng Comput* **54,** 927–937 (2016). https://doi.org/10.1007/s11517-015-1448-7

[3] MIYAJI, Masahiro. Method of drowsy state detection for driver monitoring function. *International Journal of Information and Electronics Engineering*, 2014, 4.4: 264.

[4] KOH, Sukgyu, et al. Driver drowsiness detection via PPG biosignals by using multimodal head support. In: *2017 4th international conference on control, decision and information technologies (CoDIT)*. IEEE, 2017. p. 0383-0388.

[5] LEE, Hyeonjeong; LEE, Jaewon; SHIN, Miyoung. Using wearable ECG/PPG sensors for driver drowsiness detection based on distinguishable pattern of recurrence plots. *Electronics*, 2019, 8.2: 192.

[6] MOON, Byoung-Joon, et al. Drowsy driving detection algorithm using a steering angle sensor and state of the vehicle. *전자공학회논문지 IE*, 2012, 49.2: 30-39.

[7] MEDEIROS, Jose Miguel. *Development of a heart rate variability analysis tool*. 2010. PhD Thesis.

[8] Stages of Sleep - Sleep Foundation. *Sleep Foundation* https://www.sleepfoundation.org/how-sleep-works/stages-of-sleep

[9] Sleep Cycle - POLYPHASIC SLEEP | Sleep Right, Live Well. *POLYPHASIC SLEEP | Sleep Right, Live Well* https://www.polyphasic.net/sleep-cycle/

[10] Stages of Sleep | Michigan Medicine. *University of Michigan | Michigan Medicine*. https://www.uofmhealth.org/health-library/hw48331

[11] ECG test - Better Health Channel. *Better Health Channel - Better Health Channel*. https://www.betterhealth.vic.gov.au/health/conditionsandtreatments/ecg-test

[12] CONTRIBUTORS TO WIKIMEDIA PROJECTS. Electrocardiography - Wikipedia. *Wikipedia, the free encyclopedia*. https://en.wikipedia.org/wiki/Electrocardiography

[13] BURGESS, Helen J., et al. Estimating cardiac autonomic activity during sleep: impedance cardiography, spectral analysis, and Poincare plots. *Clinical Neurophysiology*, 2004, 115.1: 19-28.

[14] MIYAJI, Masahiro. Method of drowsy state detection for driver monitoring function. *International Journal of Information and Electronics Engineering*, 2014, 4.4: 264.

[15] MHS, Carmel Armon, MD, MSc. Polysomnography: Overview, Parameters Monitored, Staging of Sleep. *Diseases & Conditions - Medscape Reference.* https://emedicine.medscape.com/article/1188764-overview

[16] CONTRIBUTORS TO WIKIMEDIA PROJECTS. Polysomnography - Wikipedia. *Wikipedia, the free encyclopedia* .https://en.wikipedia.org/wiki/Polysomnography

[17] What Does Polysomnography Involve? *News-Medical.net.* https://www.news-medical.net/health/What-Does-Polysomnography-Involve.aspx

[18] Groppo, S., Armengaud, E., Pugliese, L., Violante, M., & Garramone, L. (2020, May). Automatic Detection and Prediction of the Transition Between the Behavioural States of a Subject Through a Wearable CPS. In *International Forum on Advanced Microsystems for Automotive Applications* (pp. 177-185). Springer, Cham.

[19] SCHIFONE, Cosimo. *A robust control approach to the problem of the sea wave energy conversion*. 2020. PhD Thesis. Politecnico di Torino.